Pluronic mediated copper nanoparticles as photocatalyst for dye degradation

4.1: Introduction

The use of metals as catalysts in a variety of organic reactions and applications is a well-established approach that has been carried out efficiently for many decades [1-3]. Among many approaches to consideration of metallic compounds, metal nanoparticles (MNPs) have gained specific attention because of their physico-chemical behavior, which is very different [4, 5]. Particularly transition metals or metal oxide nanoparticles have attracted notable attention for various catalytic applications as the better alternative to costly and rare metals [6, 7]. Copper (Cu) and its oxides in this transition metal group have received significant attention due to their low cost and intriguing physico-chemical properties [8-11]. Owing to Cu metal's oxidation states (e.g., Cu^{0}, Cu^{+1}, and Cu^{+2}), environmental friendliness, and the achievable morphology in the fabrication method, Cu-based nanomaterials are widely exploited in the field of catalysis [12, 13]. Therefore, various synthetic paths have been reported for the copper nanoparticles (CuNPs) fabrication, which include the aqueous chemical reduction, thermal/vapour decomposition, laser ablation, precipitation, micro-emulsion, sol-gel, electrochemical, electrospinning, and microwave-based techniques [14-23]. Even though many synthetic approaches have been developed, the fabrication of pure and stable CuNPs is a challenging task even present time too due to the higher susceptibility of Cu to oxidation compared with precious gold (Au) and silver (Ag) nanoparticles [24-26].

The microwave technique for fabrication of CuNPs has promoted a special interest as it's simple, quick, economical, and favorable for large-scale nanoparticle production. Microwave irradiation gives rapid and uniform heating throughout the sample, creating hotspots and enhancing reaction kinetics. Microwave heating leads to faster and more controlled reactions, allowing nanoparticle formation in a shorter time. Nasser et al. [27] synthesized the CuNPs with 45 to 48 nm particle sizes using the different-different Cu salts via microwave method and found better photocatalytic activity for the reduction of safranin dye. Philip et al. [28] also successfully utilized the microwave-irradiation for fabrication of fcc structured CuNPs using the leaf extract 'Psidium guajava' as stabilizing agent and applied for in-vitro antioxidant and antimicrobial potency. Similarly, Baldi et al. [29] also synthesized CuNPs using polyol as a reducing agent and the microwave-irradiation method, which showed the better optical properties of colloidal CuNPs. As per the literature survey, it was found that the research work on the preparation of CuNPs

through the microwave technique is still not much exploited, so we also applied this non-hazardous method for CuNPs fabrication in the present research.

For the fabrication of MNPs, various types of template-supported approaches have also been used in the classes of hard and soft. Monodispersed silica [30], iron oxide nanocrystals [31], and even AuNPs [32] are examples of hard templates, whereas soft templates generally consist of microemulsion droplets [33] and polymeric micelles [34, 35]. Normally optical, electronic, and catalytic properties of MNPs are highly relying on their size, shape, and composition. Amphiphilic polymers serve as the supporting materials that form the polymeric micelles, which are used to cap or incorporate MNPs in order to fabricate the desired structure and be more stable when physico-chemical changes happen [36]. Amphiphilic polymer can interact with the metal precursor and the solvent in which the synthesis is taking place since it contains both hydrophobic and hydrophilic components. The hydrophobic part of the polymer can interact with the metal precursor, while the hydrophilic part can interact with the solvent. This interaction can prevent the metal particles from aggregation, which can lead to nanoparticles with desired properties [37, 38]. Previously, Sakai and Alexandridis synthesized AuNPs in a single step using Pluronics as stabilizing, morphogenic, and reducing agents [39, 40]. Pluronic forms core-shell micelles with a POP core and a POE shell above the CMT (critical micellar temperature) and the CMC (critical micelle concentration) [41]. The PPO part of the Pluronic can interact with the metal precursor, while the PEO part with the solvent which can prevent the nanoparticles from aggregation and leading to synthesize nanoparticles with required properties. Pluronic can be used as reducing agents, which can help turn the metal precursor into nanoparticles. The polymer's ability to reduce can be boosted by the PPO part, which can help increase the quantity of the metal precursor near the polymer. This makes it easier for the polymer to reduce [40, 42, 43]. The CuNPs obtained using Pluronic polymers as reducing and/or stabilizing agents have been reported by chemical reduction and photo-assisted paths and found the particle size range between 10-50 nm [44, 45]. Therefore, we also considered these Pluronic polymers for our purpose of fabricating CuNPs for its better applications in the removal of hazardous materials.

Most of the organic dyes employed in the textile, paint, pharmaceutical, and plastics industries are not biodegradable and are very bad for the environment. The dyes that come out of the textile and dying industries are bad for the environment because they leave behind long-lasting colors

and put too much COD in the water. Up to 20% of all manufactured dyes are estimated to disappear during the dyeing treatment and end up in the water bodies through effluents [46]. To address critically this problem, researchers have employed a number of physico-chemical methods, including adsorption, coagulation, flocculation, and membrane-filtration [47-49]. However, such methods are used to separate organic dyes from effluents but do not degrade them [50]. Not only that, they are inefficient and high-cost approaches, producing many byproducts that also require processing from an environmental point of view [51]. In the last few years, MNPs of multiple compositions, size, structure, and morphology have been synthesized to work as photocatalysts for the organic dye degradation of owing to their facile synthetic processes and notable optical properties [52, 53]. Not only that, the use of MNPs for photocatalytic reduction of organic dyes is widely preferred as low cost and efficient and also form the biodegradable end products like amines, which microbes can easily degrade [54]. In the present study, we were performed the degradation of most widely used four common organic dyes like anionic congo red (CR) and methyl orange (MO), cationic methylene blue (MB) and rhodamine B (RhB) dyes.

CR is a water-soluble anionic azo dye and is known for its toxicity [55]. CR has carcinogenic effects and has been used mainly in the textile, plastic, and paper industries [56, 57]. It dyes cotton directly and doesn't break down well because it was made synthetically to resist fading, making it non-biodegradable. Second MO is a typically anionic dye compound that has been hugely applied in the textile, food, printing, and pharmaceutical industries [58]. The third polluting cationic dye, MB, is also extremely toxic and causes breathing problems, excessive sweating, eye injury, mental depression, and methemoglobinemia [59, 60]. The fourth common dye, RhB, is a synthetically manufactured cationic xanthene-based dye and is mainly exploited by the paper industry for printing and textiles as colorant products [61]. This heterocyclic dye is very harmful to humans and animals because it causes irritation to the eyes, skin, and respiratory tract [62]. Finally, research into the degradation of such hazardous organic dyes using MNPs is an important task at present time from textile effluents.

In this concern, our aim of this present research was to fabricate CuNPs that have a small size range, uniformity, better stability, and potent photocatalytic activity to degrade hazardous organic dyes with high efficiency. To achieve our goal, a novel microwave-assisted, Pluronic mediated synthesis of copper nanopowder and nanodispersions is developed. We created

Pluronic mediated CuNPs with sodium borohydride ($NaBH_4$) as a reducing agent and different hydrophilic Pluronics (L121, P123, and F127) as micellar reaction media using microwave-irradiation techniques. The effects of microwave-irradiation on the synthesis of Pluronic mediated CuNPs have been examined. The dispersion and powder form of fabricated Pluronic mediated CuNPs are characterized using UV-Vis fluorescence, DLS, Zeta potential, rheology, XRD, TEM, FE-SEM, and EDX measurements. The role of hydrophilicity of used Pluronics in the particles size, shape, and stability has been evaluated. The photocatalytic activity of dispersions of blank CuNPs and Pluronic F127 mediated CuNPs for the degradation of common CR, MO, MB, and RhB organic dyes under sunlight irradiation have been investigated, and their reaction mechanism has been proposed.

4.2: Experimental section

4.2.1: Fabrication of the blank CuNPs and Pluronic mediated CuNPs

The CuNPs were fabricated using a facile, single-pot, microwave-assisted method. The synthesis was done through the modified typical method of the wet-chemical reduction using microwave heating, $NaBH_4$ as reducing agent, and Pluronic micellar solutions as the solvent. The fabrication process is presented in Figure 4.1(a).

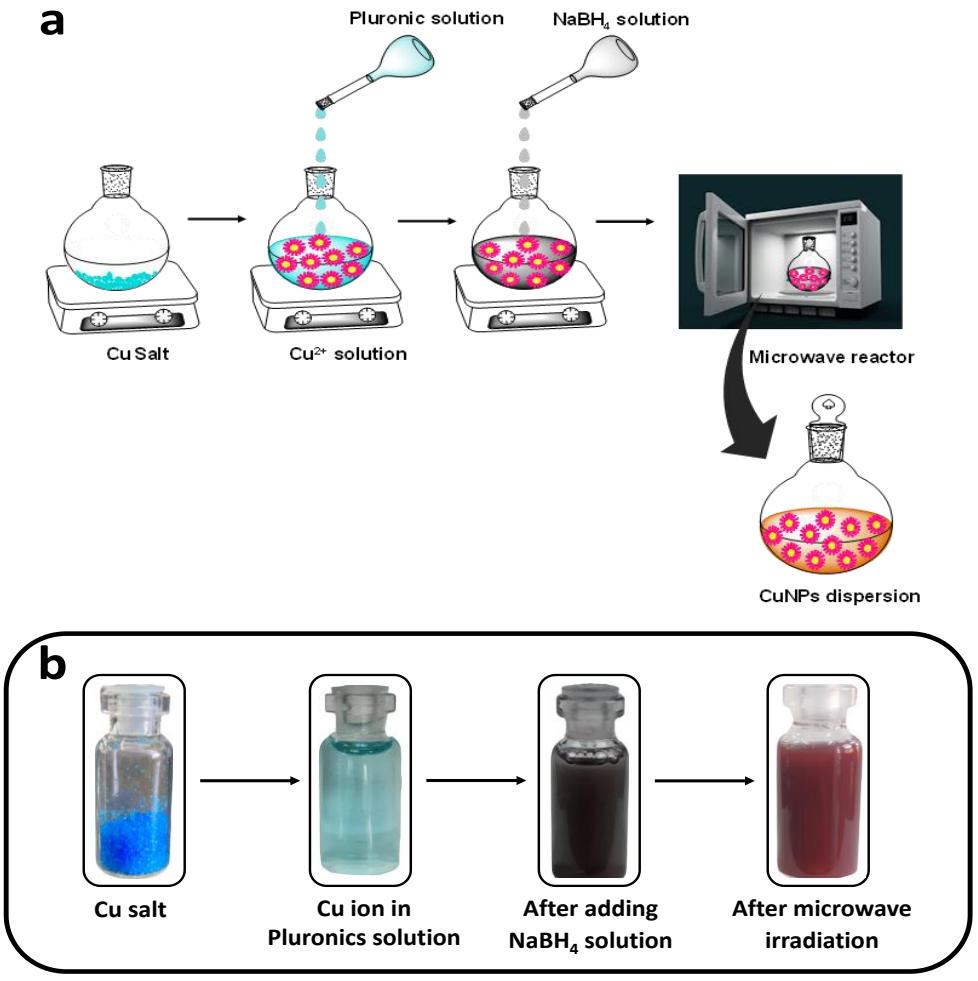

Figure 4.1: (a) Fabrication of the Pluronic mediated CuNPs using microwave technique. (b) Colour alteration during the CuNPs fabrication.

Here, a typical 0.1 M $CuSO_4 \cdot 5H_2O$ solution was prepared with and without 2 wt% Pluronic micellar solution in a 250 mL three-necked RBF. With fine stirring at 450 rpm, a 0.2 M $NaBH_4$

solution was made and added to the copper solution. Here, the color of the solution turns black because of the surface plasmon resonance (SPR), which results from the absorption of specific wavelengths of light in the visible spectrum due to the size and shape of particles during the initial reduction process. The resulting mixture was immediately exposed to microwave-irradiation (StartSYNTH microwave oven, MilstoneSrl, Italy) at 350 W power and 50 Hz energy level for different time intervals (1, 3.5, 5, 7.5, 10, and 12.5 min) at 70 °C temperature. The color of the colloidal solution turned red-ochre when nanoparticles formed. The dispersions of red-emitted CuNPs were then analyzed for optimization of the microwave-irradiation time and other required experiments. For solid state characterization, the CuNPs solution was cooled, centrifuged (2000 rpm) for 20 min, filtered, and washed with ultrapure water and ethanol. This turned the solution into a CuNPs powder. Finally, the solid CuNPs were dried in a lab oven at 90 °C for 2 h. The dark reddish brown color powder of CuNPs was stored at RT for further study. The composition, condition, and code names of fabricated Pluronic mediated CuNPs have been shown in Table 4.1. The blank CuNPs were fabricated in the same manner without using Pluronic micellar medium.

Table 4.1: Composition and code-names of fabricated CuNPs.

Cu salt concentration (M)	$NaBH_4$ concentration (M)	Pluronic used	Concentration of Pluronic fixed (wt%)	Microwave-irradiation optimized (min)	Code-name of CuNPs
0.1	0.2	---	---	10	blank CuNPs
0.1	0.2	L121	2.0	7.5	CuNPsL1
0.1	0.2	P123	2.0	7.5	CuNPsP3
0.1	0.2	F127	2.0	7.5	CuNPsF7

4.2.2: Photocatalytic organic dye degradation studies

The reductive degradation of common organic dyes likes CR, MO, MB, and RhB was examined using the fabricated blank CuNPs and Pluronic F127 micelles-mediated CuNPs (CuNPsF7) dispersions as photocatalysts. In a beaker, 50 mL of each dye solution (15 ppm) was mixed with 4 mL of CuNPs dispersion and stirred in dark for an hour to manage absorption-desorption equilibrium. After that, the1 mL of 0.1 M $NaBH_4$ solution was added to the dispersion mixture and stirred. The dispersion mixture was then exposed to sunlight (Intensity in the range of 875–

900 W/m^2) from 12.00 noon to 3.30 p.m. The temperature during the experiments was in the range of 32° to 34 °C in Vadodara (the central zone of Gujarat) in India. At a specific time interval, aliquots were withdrawn out of the beaker and directly analyzed through a UV-Vis spectrophotometer (UV-1900, Shimadzu, Japan). The kinetics of the dye's photocatalytic degradation was also investigated. The following Eq. (1) is used to determine the percentage degradation of the organic dye using the blank CuNPs and CuNPsF7 as photocatalysts.

$$\% \text{ Degradation} = [(C_0-C_t)/C_0] \times 100 \quad \text{---------- (1)}$$

Here, the dye initial concentration before sunlight exposure is considered as C_0, and the dye concentration after sunlight irradiation at time t is C_t.

4.3: Results and discussion

4.3.1: Characterization of the blank CuNPs and Pluronic mediated CuNPs

4.3.1.1: Optical characterization of the CuNPs dispersions

First, we fabricated CuNPs without Pluronic micelles mediation in water using the microwave-assisted technique by chemical reduction of an aqueous Cu^{2+} salt solution with reducing agent $NaBH_4$. The CuNPs formation was clearly evidenced by the color changes occur in solution from sky-blue to red-ochre (Figure 4.1(b)). In general, the microwave-irradiation time has strongly influenced on the fabrication and particle size of the CuNPs. Microwave irradiation uniformly heats the reaction mixture, overcoming mass transfer restrictions and promoting nanoparticle nucleation. This can produce smaller, monodisperse nanoparticles with enhanced characteristics for various applications [63-67]. The fluorescence spectrums of fabricated blank CuNPs solutions applying varied microwave-irradiation times (1, 3.5, 5, 7.5, 10, and 12.5 min) were recorded for the purpose of optimization of irradiation time and are shown in Figure 4.2.

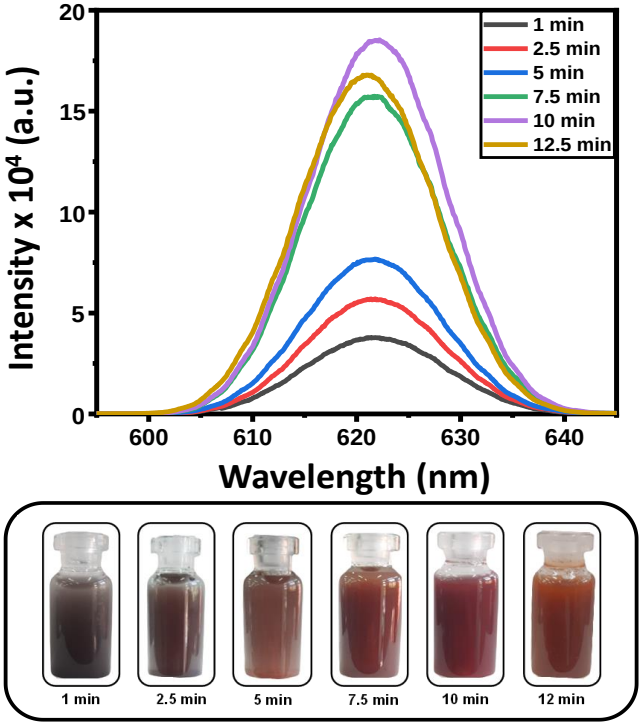

Figure 4.2: (a) Fluorescence spectrums of the blank CuNPs fabricated at various microwave-irradiation time. (b) Color alteration during the fabrication of CuNPs.

Results shown in the spectra of blank CuNPs in Figure 4.2(a) clearly indicated that the intensity was higher at 10 min of microwave-irradiation time, which was considered the optimized period

for fabrication. The steady-state fluorescence emission spectra of fabricated CuNPs in the aqueous micellar solutions of different Pluronics (L121, P123, and F127) after applying varied microwave-irradiation times (1, 3.5, 5, 7.5, 10, and 12.5 min) were also recorded (shown Figure 4.3 to 4.6). The fixed 2 wt% concentration of all the Pluronics has been taken into consideration as per their CMC when set as a micellar medium. Here, Figure 4.7(a) shows the plot of emission intensity versus microwave-irradiation time for the fabricated Pluronic mediated CuNPs dispersions. The optimized microwave-irradiation time for CuNPs in Pluronic micellar solutions was 7.5 min, which was less than the time for CuNPs in the absence of Pluronic micellar solutions. Microwave irradiation can provide rapid and efficient heating to the reaction mixture, which can lead to fast reaction rates and short reaction times, which can improve the yield and size of the nanoparticles [64].

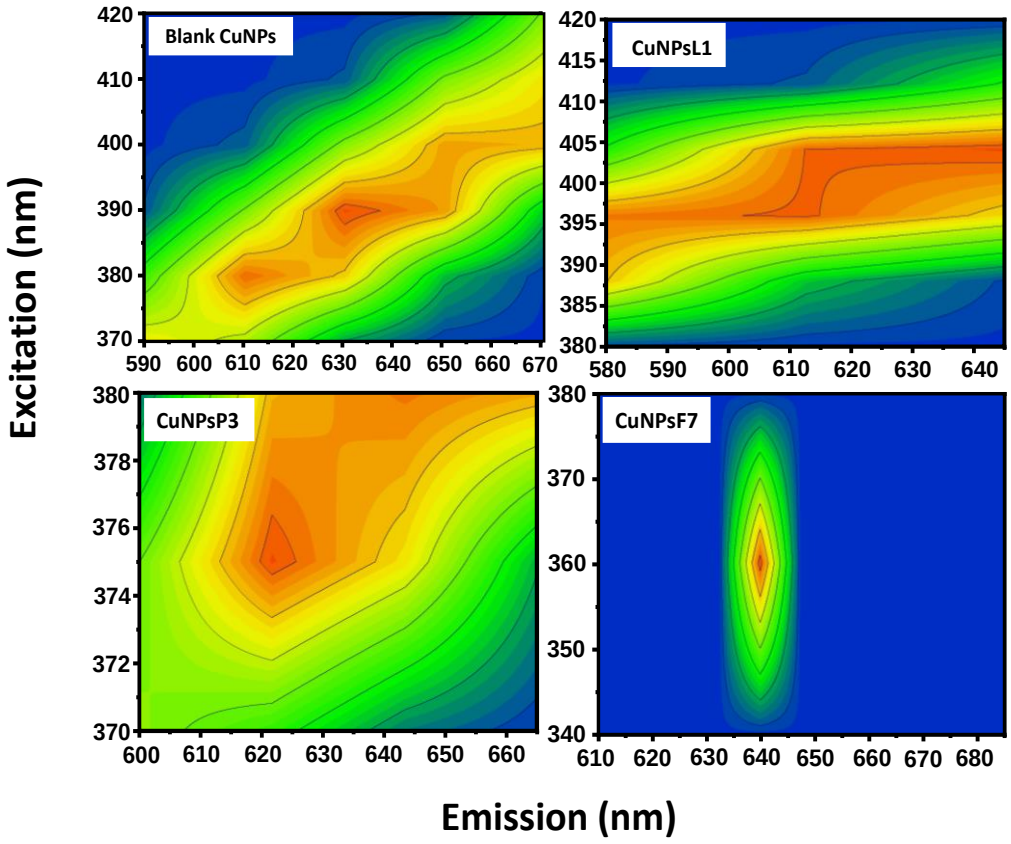

Figure 4.3: Emission-excitation spectra of blank CuNPs and Pluronic mediated CuNPs.

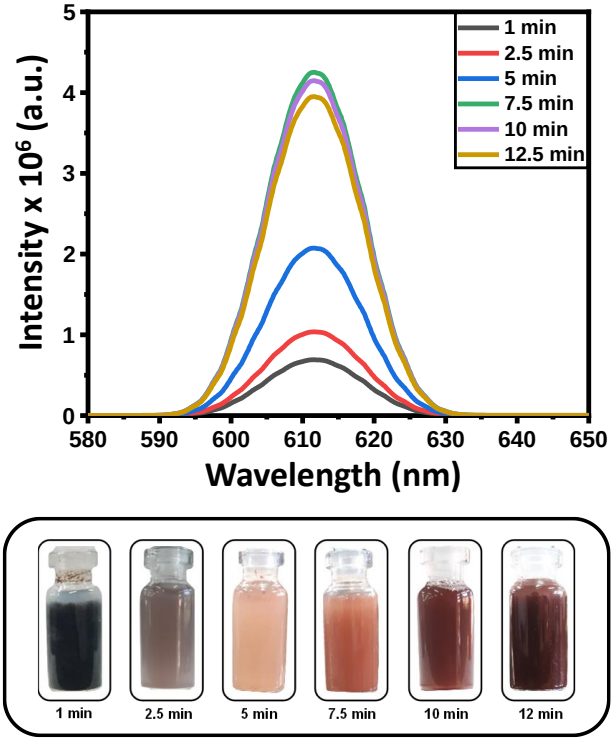

Figure 4.4: Steady state fluorescence spectrums of the CuNPsL1 fabricated at various microwave irradiation time.

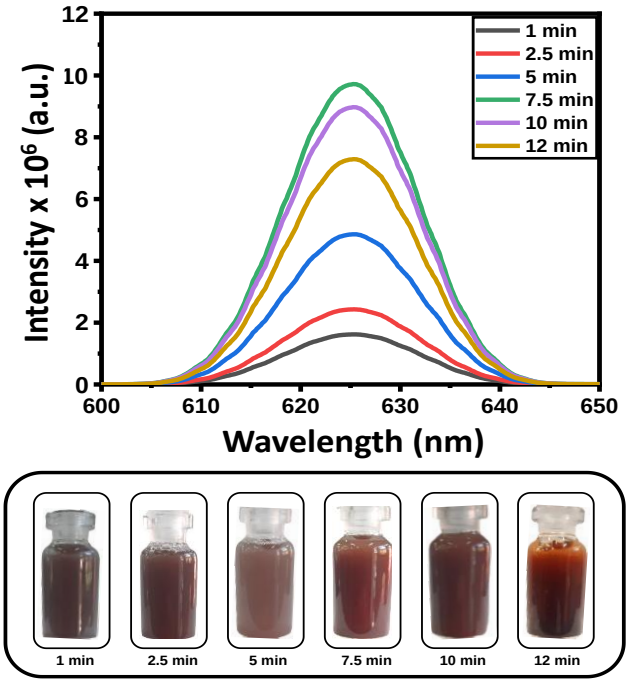

Figure 4.5: Steady state fluorescence spectrums of the CuNPsP3 fabricated at various microwave irradiation time.

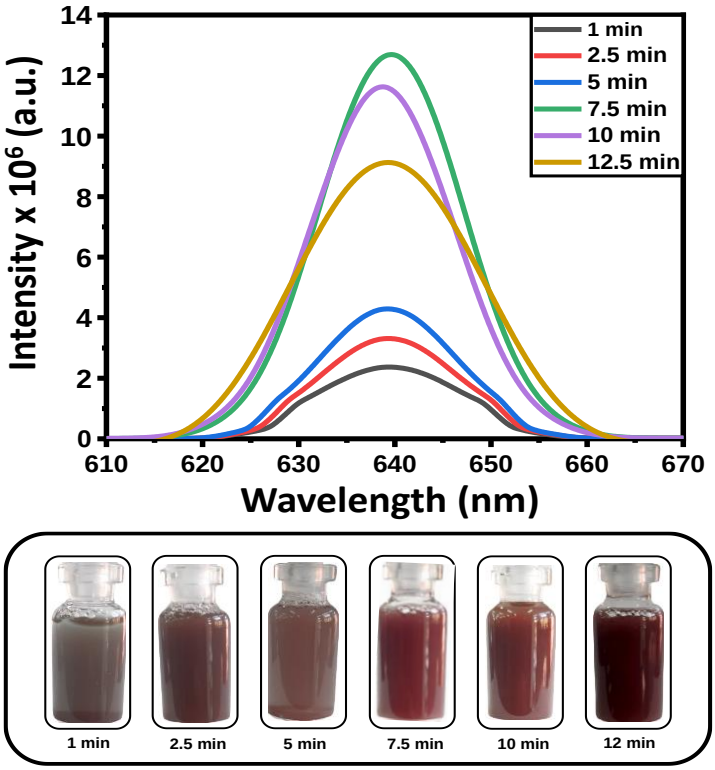

Figure 4.6: Steady state fluorescence spectrums of the CuNPsF7 fabricated at various microwave irradiation time.

Here, the Pluronic molecules along with water molecules could also be excited by microwave-irradiation, which would also speed up the reduction rate of Cu^{2+} and form nanoparticles. In the case of Pluronic micellar solutions, the Cu^{2+} ions are bound to the PEO and PPO parts of Pluronic molecules and reduced to Cu^{0} through iondipole interactions in between the Cu^{2+} and the lone pair electrons of the ethereal oxygen present in the linkages [68]. Therefore, several oxygen atoms present in the PEO and PPO chains of Pluronic interact with metal ions like many PEO-structured polymers, mainly responsible for the reduction of metal ions at quick time [69,70]. It is also seen that the emission intensity was higher in the CuNPsF7 than in the other two CuNPsP3 and CuNPsL1 at the optimized 7.5 min microwave-irradiation time.

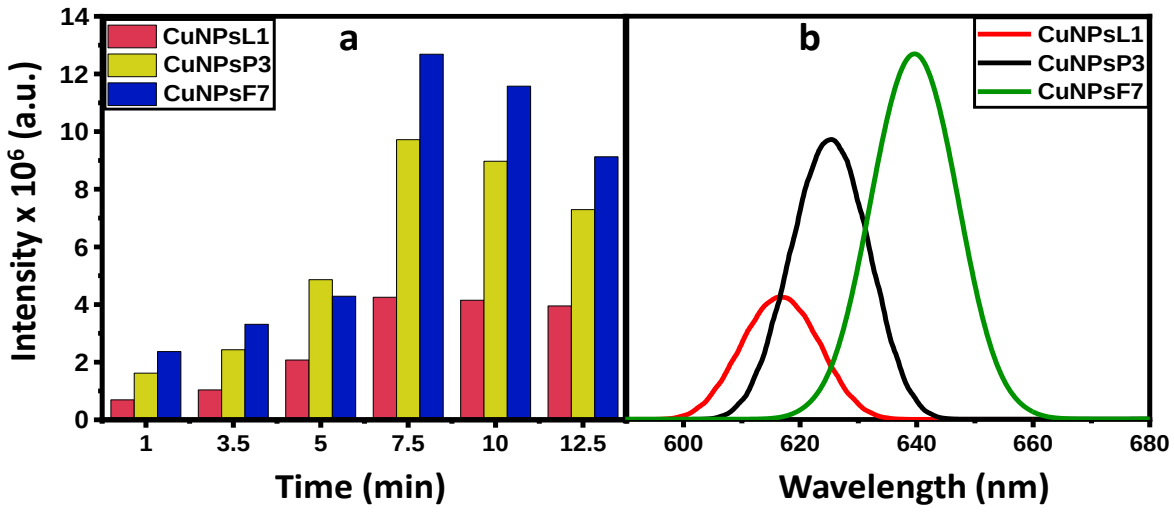

Figure 4.7: (a) Optimized period of microwave-irradiation for the Pluronic mediated CuNPs. (b) Fluorescence spectrums of Pluronic mediated CuNPs at 7.5 min microwave-irradiation.

To clarify this performance of CuNPsF7, we also showed the steady-state fluorescence spectra of Pluronic mediated CuNPs with different hydrophilicity of Pluronics at RT in Figure 4.7(b). The sharp band has been observed at the wavelengths of 611.68 nm for CuNPsL1, 625.28 nm for CuNPsP3, and 639.59 nm for CuNPsF7 dispersion, respectively. A clear red shift has been noticed in the case of Pluronic mediated CuNPs. The intensity changes were found to occur in the following order: CuNPsL1<CuNPsP3<CuNPsF7. It indicated that the Pluronic with increasing hydrophilic PEO block length showed high intensity, which is consistent with an increase in reaction activity. L121 has 10 % ethylene oxide units and P123 has 30 % ethylene oxide units in its molecular structure, while F127 has 70 % ethylene oxide units, indicating that the F127 is more hydrophilic than the P123 and L121. Results clearly showed that CuNPsF7 was found to be better than CuNPsP3 and CuNPsL1 as a highly hydrophilic material and for the formation of particles with a larger nanoscale. Because of Pluronic F127 molecules extended conformation and high solubility in water, highly hydrophilic F127 can provide more efficient steric stabilization, resulting in the creation of more stable and monodisperse CuNPs. Furthermore, highly hydrophilic Pluronic F127 can have a higher density of hydroxyl groups, which can facilitate the nucleation and growth of copper nanoparticles by providing more efficient reducing and capping agents. These results are also supported by the UV-Vis absorbance spectra of the blank and Pluronic mediated CuNPs shown in the Figure 4.8,

whichclearly show the absorption peak shifted from 589 nm to 562 nm (blueshift) when the PEO part increased [71].

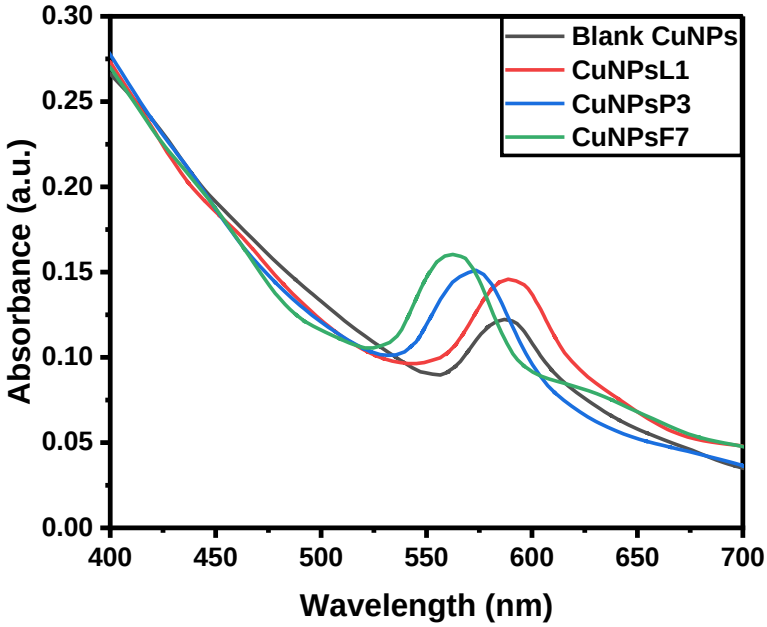

Figure 4.8: UV-Visible absorbance spectrums of the Blank CuNPs and Pluronic mediated CuNPs

4.3.1.2: Structural characterization of the CuNPs dispersions

The DLS techniques were employed to investigate the structural parameters of blank CuNPs and Pluronic mediated CuNPs dispersions. As we analyzed the nanoparticle dispersions, the particle size was measured as the hydrodynamic diameter (D_h). Size distribution curves of fabricated blank CuNPs and Pluronic mediated CuNPs dispersions at RT are shown in Figure 4.9. The D_h values of blank CuNPs, CuNPsL1, CuNPsP3, and CuNPsF7 were 48.90 nm, 113.0 nm, 26.28 nm, and 12.70 nm, respectively. The Pluronic mediated CuNPs were given much smaller particle sizes than blank CuNPs. Pluronic micelles have a high surface area per volume, which facilitates amore number of active sites for the reduction to occur. In this study, the D_h value of CuNPsF7 was found to be the smallest when compared to that of CuNPsL1 and CuNPsP3, indicating that an increase in Pluronic hydrophilicity provides a greater number of oxyethylene units for the binding of Cu^{2+} ions reduced to Cu^0 via ion-dipole interactions in between the Cu ion and the lone pair electrons of the PEO linkages [68]. The narrow size distribution and highly intense peak of CuNPsF7 confirmed the better yield of particles and the smallest size of the fabricated CuNPs. Also, the blank CuNPs, CuNPsL1, CuNPsP3, and CuNPsF7 have PDI values of 0.226,

0.234, 0.171, and 0.110, respectively. Here, the results of PDI show that as the PEO part of the Pluronic increases, the PDI value decreases. A low PDI value indicates that the particle size distribution is narrow and that particle size variation is minimal. It indicated that the particle formation was uniform in size and had a homogeneous particle size distribution [29].

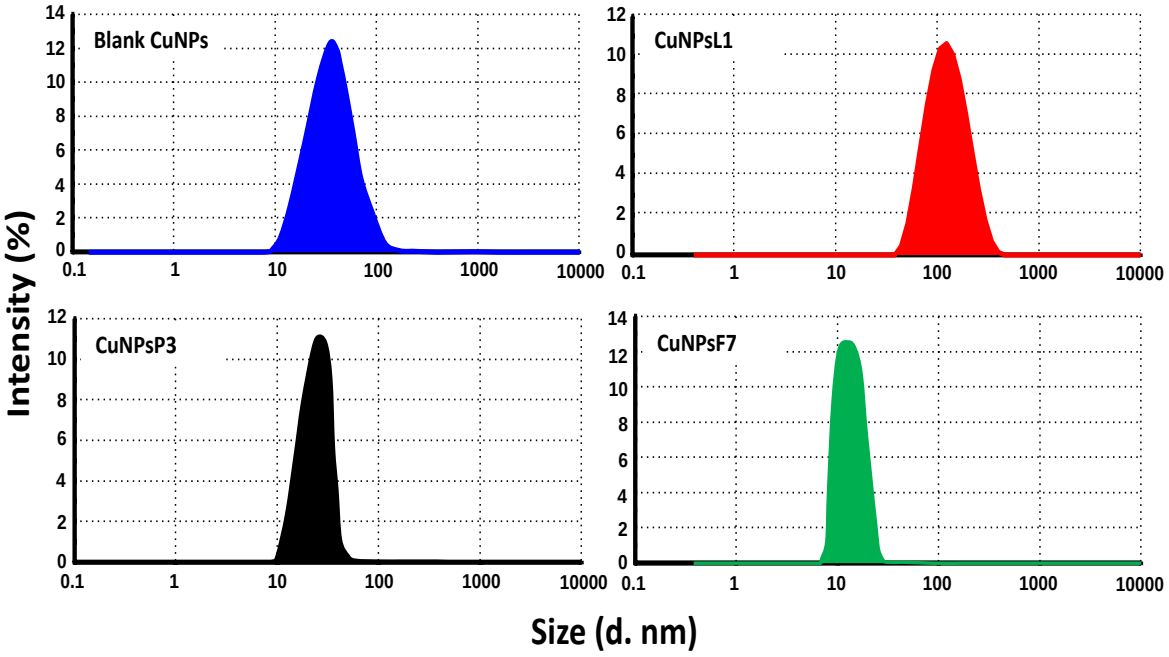

Figure 4.9: Size distribution curves of blank CuNPs and Pluronic mediated CuNPs dispersions.

The zeta potential is a recognized parameter to understand the stability of colloidal nanoparticles. The Z potential of the blank CuNPs and Pluronic mediated CuNPs dispersions was monitored and presented in Figure 4.10. The Z potential measured for blank CuNPs was -32.80 mV, which was similar with the reported value [72]. The high Z potential values clearly showed that the surface of the blank CuNPs has been covered with borohydrates ions. The Z potential values of Pluronic mediated CuNPs were in the range of -12.7 mV to -10.2 mV, which is quite lower than the -32.80 mV of blank CuNPs. The zeta potential values of CuNPs in Pluronic micellar solutions are found to be low due to the absence of charged groups on the surface of the micelles. The polymeric chains of the micelles adsorb onto the surface of the nanoparticles and prevent them from coming into close contact with each other, which can reduce their tendency to aggregate [73].

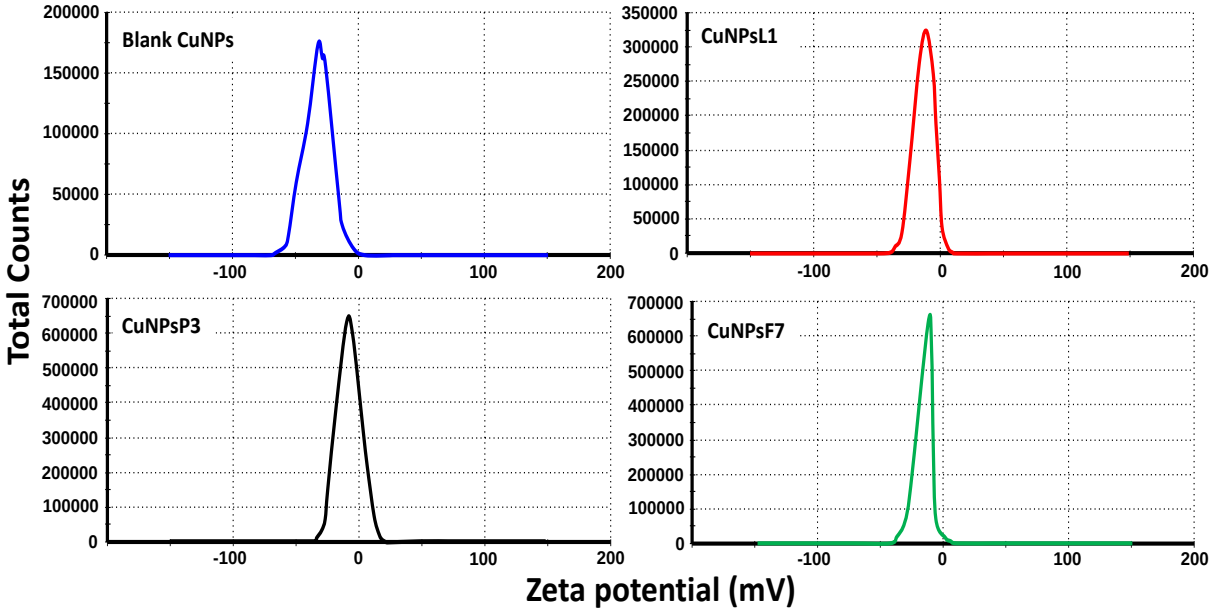

Figure 4.10: Zeta potential profile of blank CuNPs and Pluronic mediated CuNPs dispersions.

The viscosity of the Pluronic mediated CuNPs dispersions was also monitored at RT and shown in Figure 4.11. Results showed an increasing trend in the viscosity of Pluronic mediated CuNPs with increasing hydrophilicity. Results show that CuNPsF7 has the highest viscosity compared to CuNPsL1 and CuNPsP3. It's because of the use of highly hydrophilic F127 and smaller particle sizes. Pluronic mediated CuNPs were shown to exhibit non-Newtonian shear thinning characteristic at low shear rates (20 s^{-1}) which type of behavior can be beneficial for flowability in many applications [74]. However, as the shear rate increased, it became weaker and lost its non-Newtonian properties, indicating that the flow of the Pluronic mediated CuNPs dispersions is shear thickening. Hence, it was understood that the strong interaction between Pluronics and CuNPs may be due to the shear thinning nature and incremental shear viscosity between Pluronics and nanoparticles. Such rheological results proved that the CuNPsF7 nanoparticles are best used in liquid media. Hence, CuNPsF7 would be highly useful as an applicable material in the aqueous dispersion medium for its photocatalytic properties in the treatment of water or other hazardous effluents.

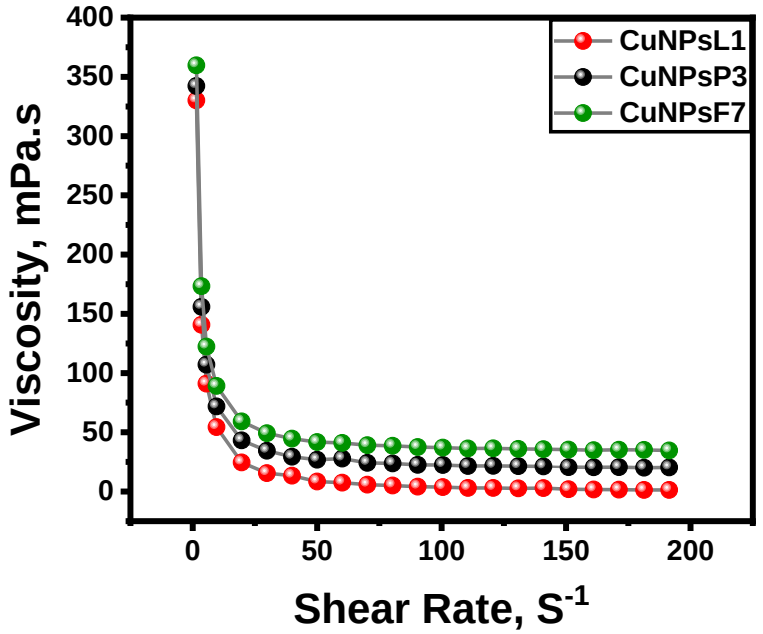

Figure 4.11: Rheological behavior of Pluronic mediated CuNPs dispersions at RT.

4.3.1.3: Solid state characterization

To figure out the particle sizes, shapes, crystallinity, and composition of the powdered form of the Pluronic mediated CuNPs, the particles were separated from colloidal dispersion through centrifugation, filtration, washing with ultrapure water, and then drying in an oven. Two electron microscopic techniques, TEM and FE-SEM, are used to figure out the morphology as well as the size of the fabricated nanoparticles. Figure 4.12 displays the TEM images of the fabricated solid blank and Pluronic mediated CuNPs. The image of blank CuNPs illustrates that when CuNPs are synthesized without adding a stabilizing agent, i.e., Pluronic, aggregated forms of particles are found rather than a uniform size, which reflects the lack of stability against the agglomeration of the particles. We have chosen Pluronic L121, P123, and F127 as stabilizing agents in the CuNPs fabrication to investigate the effect of hydrophilicity on the fabricated CuNPs. In these polymers, there is a substantial change in the PEO chain length, while the PPO chain length remains the same. The sizes of the nanoparticles have been calculated using the subscribed form of J software system. The particle size values of blank CuNPs, CuNPsL1, CuNPsP3, and CuNPsF7 were 42.35 nm, 64.83 nm, 32.43 nm, and 7.40 nm, respectively.

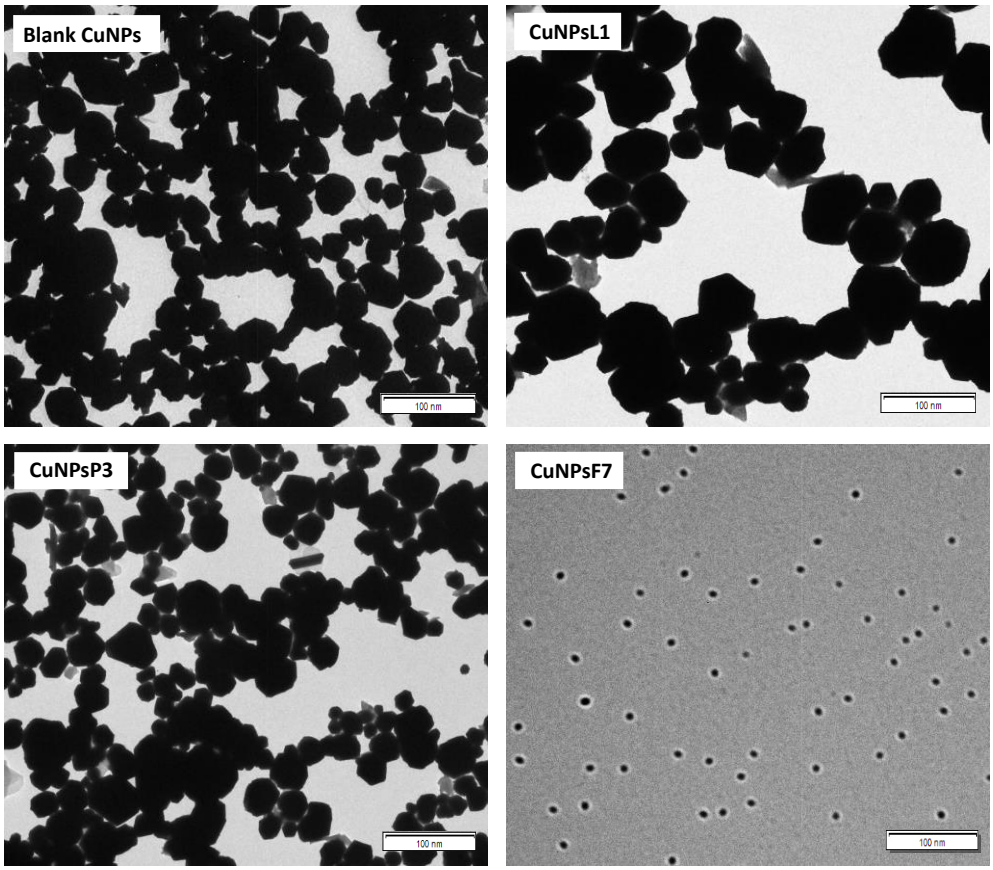

Figure 4.12: TEM images of blank CuNPs and Pluronic mediated CuNPs.

The particle size of the TEM images of CuNPsL1 clearly showed non-uniform and bulky-sized particles with more than 60 nm, while the other two, CuNPsP3 and CuNPsF7, showed better morphology and nano sizes. As it was clear, L121 has low HLB and, due to the short PEO chain length, is unable to show better formation of micelles at applied condition, which is proven by the maximum D_h (113.0 nm) in DLS analysis and high size of 64.83 nm through TEM. Hence, a significant amount of particle agglomeration is observed in CuNPsL1 [75]. On the other hand, P123 and F127 have significantly higher HLB values and cloud points, and so they readily form core-shell micelles at ambient temperatures to control the formation of CuNPs. Both the CuNPsP3 and the CuNPsF7 were shown to be quite uniform in their sizes and cubic shapes. Nevertheless, a good amount of aggregation in comparison to CuNPsF7 is also observed with CuNPsP3. But the TEM image of CuNPsF7 showed quite small and uniform particles with cubic morphology. Results highlighted that the CuNPsF7 with significantly higher PEO chain segments are suitable to overcome the problem of CuNPs aggregating or growing further by

stabilizing them through steric hindrance or electrostatic repulsion and have a low 7.40 nm particle size and cubic morphology

The observations of the TEM analysis were given support by the FE-SEM analysis of the fabricated blank CuNPs and Pluronic mediated CuNPs (shown in Figure 4.13). Like TEM, the blank CuNPs had morphology with larger sizes due to agglomerated forms and a little bit of a convincing cubic shape. The CuNPsL1 showed non-uniformity in sizes. Both CuNPsP3 and CuNPsF7 displayed convincing cubic morphology with well-uniform particle sizes. The TEM and FE-SEM images show a homogeneous particle size distribution, confirming the low PDI value (shown in DLS results) of uniformly sized particles. These results could be attributed to the significance of the longer PEO chain lengths of F127, which play the role of defeating the susceptibility of CuNPs towards agglomeration and display the smallest sizes with uniform dispersion. Due to the better solubility of Pluronic F127 micelles, they can provide more efficient steric stabilization, resulting in the creation of more stable and monodisperse CuNPs [76]. Of course, the CuNPs will continue to grow outward from the micelles as time passes.

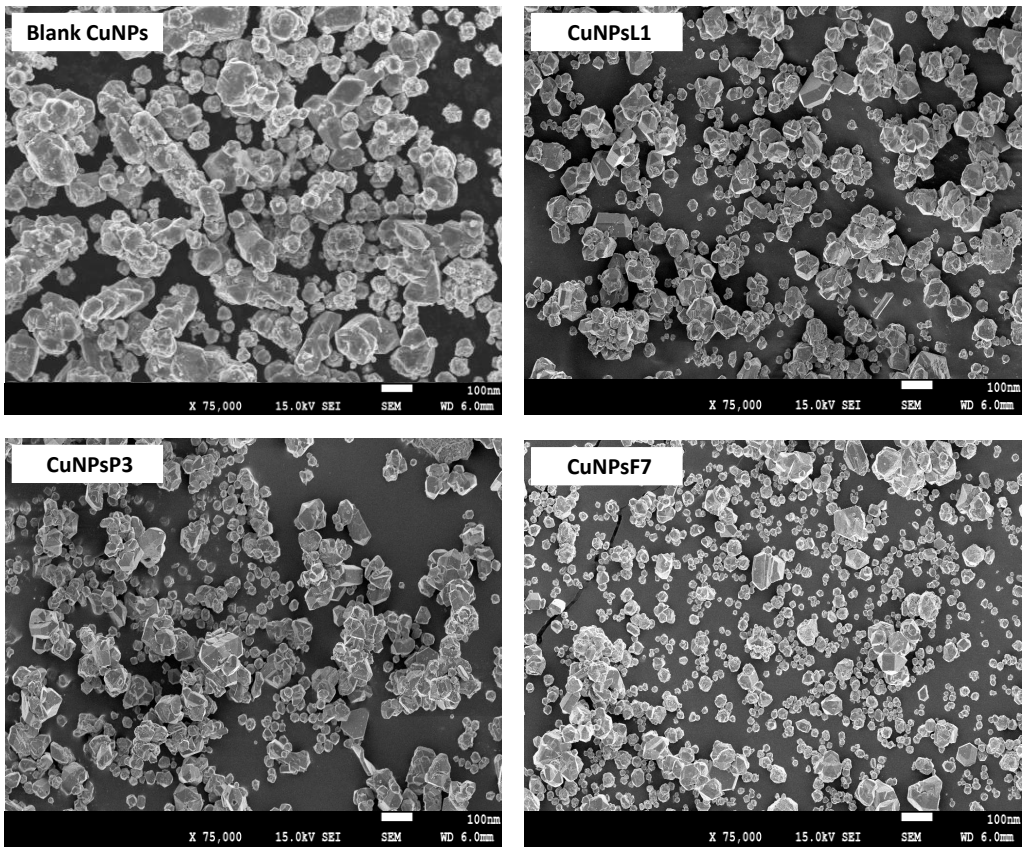

Figure 4.13: FE-SEM images of the CuNPs and Pluronic mediated CuNPs.

Figure 4.14 shows the XRD spectra of blank CuNPs and Pluronic mediated CuNPs. The blank CuNPs showed sharp peaks at 43.59°, 50.81°, and 74.49° (2θ values), which are analogous to the (111), (200), and (220) lattice planes, and all these three peaks are matched with the fcc (face-centered cubic) metallic Cu as per the JCPDS Card No. 04-0836 for the fcc metallic Cu. Here, the peaks at 43.19°, 50.68°, and 74.36° for CuNPsL1, 43.32°, 50.55°, and 74.23° for CuNPsP3, and 43.46°, 50.41°, and 74.09° for CuNPsF7 are also identical to the (111), (200), and (220) lattice planes of fcc metallic Cu [77]. All the calculating parameters of the analysis are shown in the Table 4.2. It was observed that all the fabricated Pluronic mediated CuNPs met the fcc structure with a highly crystalline nature in their solid form. It was also observed that no additional peaks were observed, demonstrating the absence of any CuO or Cu_2O in the fabricated nano copper.

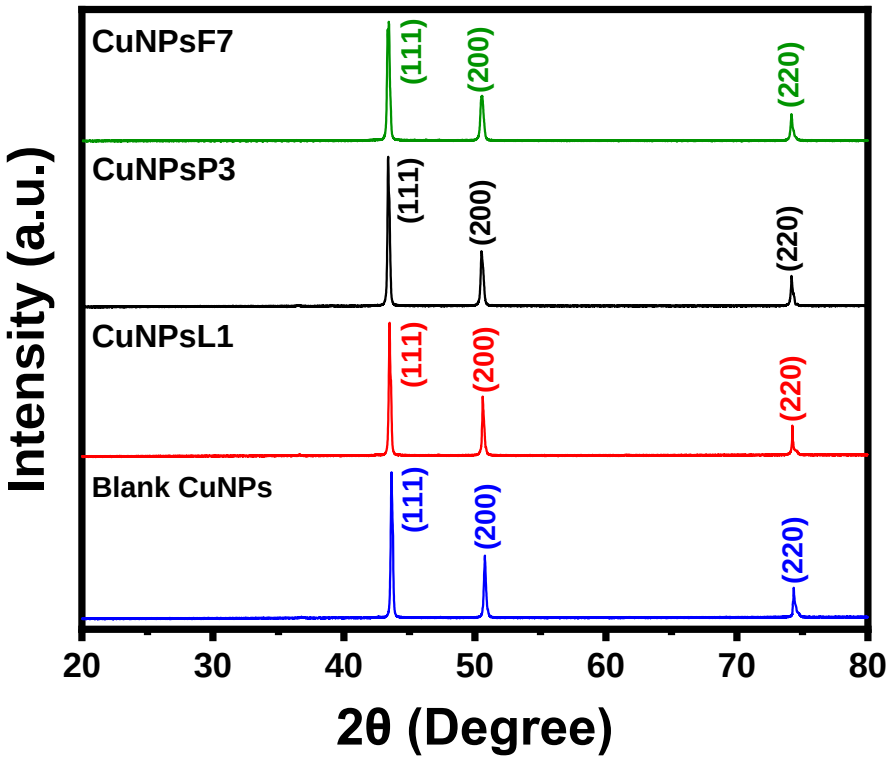

Figure 4.14: XRD patterns of the blank CuNPs and Pluronic mediated CuNPs.

From XRD study, considering the peak at degrees, average particle size has been estimated by using Debye-Scherrer formula.

$$D = \frac{0.9\,\lambda}{\beta \cos\theta} \quad \text{.....……..... (1)}$$

Where 'λ' is wave length of X-Ray (0.1541 nm), 'β' is FWHM (full width at half maximum), 'θ' is the diffraction angle and 'D' is particle diameter size.

Calculation of d-Spacing:

The value of d (the interplanar spacing between the atoms) is calculated using Bragg's Law:

$$2d\sin\theta = n\lambda \quad \ldots\ldots\ldots\ldots\ldots\ldots (2)$$

Table 4.2: The calculated parameters of Pluroinic-mediated CuNPs

Nanoparticles	2θ value	d spacing nm	Standard d spacing nm	h k l
Blank CuNPs	43.65279	0.2017	0.2078	111
	50.76582	0.1749	0.1800	200
	74.8396	0.1234	0.1274	220
CuNPs in L121	43.50514	0.2023	0.2078	111
	50.63096	0.1753	0.1800	200
	74.24634	0.1242	0.1274	220
CuNPs in P123	43.40872	0.2028	0.2078	111
	50.5473	0.1756	0.1800	200
	74.20219	0.1243	0.1274	220
CuNPs in F127	43.40325	0.2028	0.2078	111
	50.54062	0.1756	0.1800	200
	74.18931	0.1243	0.1274	220

The value of lattice constant "a" is calculated using below formula:

$$a = d_{hkl}\sqrt{h^2 + k^2 + l^2} \quad \ldots\ldots\ldots\ldots (3)$$

The values for the lattice constant were found 3.60 a Å for all the fabricated CuNPs.

Similar observations have also been found in the EDX analysis of the fabricated CuNPs and Pluronic mediated CuNPs (displayed in Figure 4.15). EDX analyses showed a very homogenous high copper composition for all the CuNPs, with a purity of 85-95 % copper. No oxygen was seen, confirming the absence of copper oxides. With a composition of 93.39 % Cu in the fabricated CuNPsF7, Pluronic F127 micelles proved its effectiveness as a stabilizing agent in the microwave-assisted CuNPs fabrication.

Overall characterization and properties studies of the fabricated Pluronic mediated CuNPs have led to the conclusion that the CuNPsF7 may be potent nanomaterials for applications as they

have the smallest size, better homogeneity, high stability, excellent copper particle composition, and good compatibility in the medium.

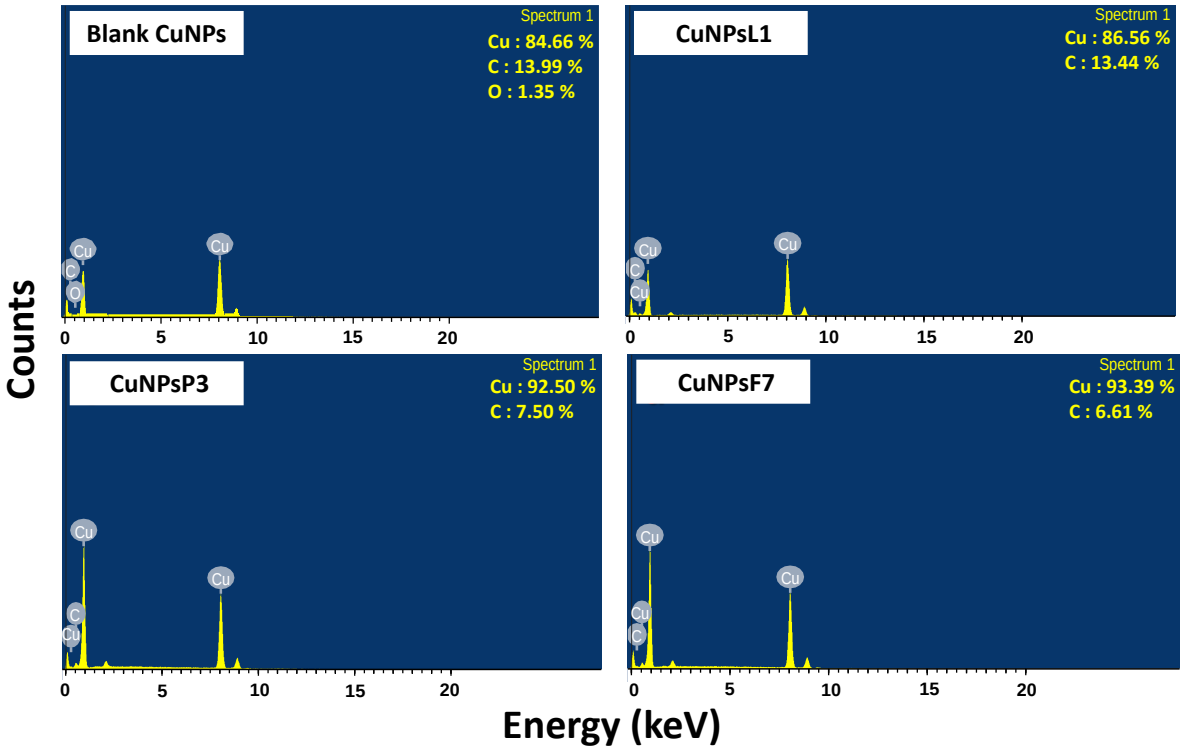

Figure 4.15: EDX spectra of blank CuNPs and Pluronic mediated CuNPs

4.3.2: Photocatalytic activity of the blank CuNPs and Pluronic mediated CuNPs

Based on the complete characterization of the Pluronic mediated CuNPs, our results showed that the Pluronic F127 micelles mediated CuNPs (CuNPsF7) with the smallest size, highest stability, and most copper-rich phase should be used as photocatalysts for their better applications.

The photocatalytic activity of the blank CuNPs and CuNPsF7 using microwave techniques was evaluated through the photocatalytic degradation of four common usable organic dyes (i.e., anionic CR & MO and cationic MB &RhB) under sunlight irradiation. The photolysis of dyes under sunlight irradiation in the absence of any kind of nanoparticles was found insignificant for an almost 200 min time period shown Figure 4.16. It clearly indicates that there are no possibilities for any kind of degradation or reduction. But the intensity of these organic dyes was gradually reduced in the presence of the added $NaBH_4$. Here, the degradation rate for each dye was determined using Eq. 1. Figure 4.17 shows the maximum % dye degradation in the presence

of $NaBH_4$, which was determined as 13.30 % for CR, 11.03 % for MO, 15.18 % for MB, and 14.69 % for RhB, respectively.

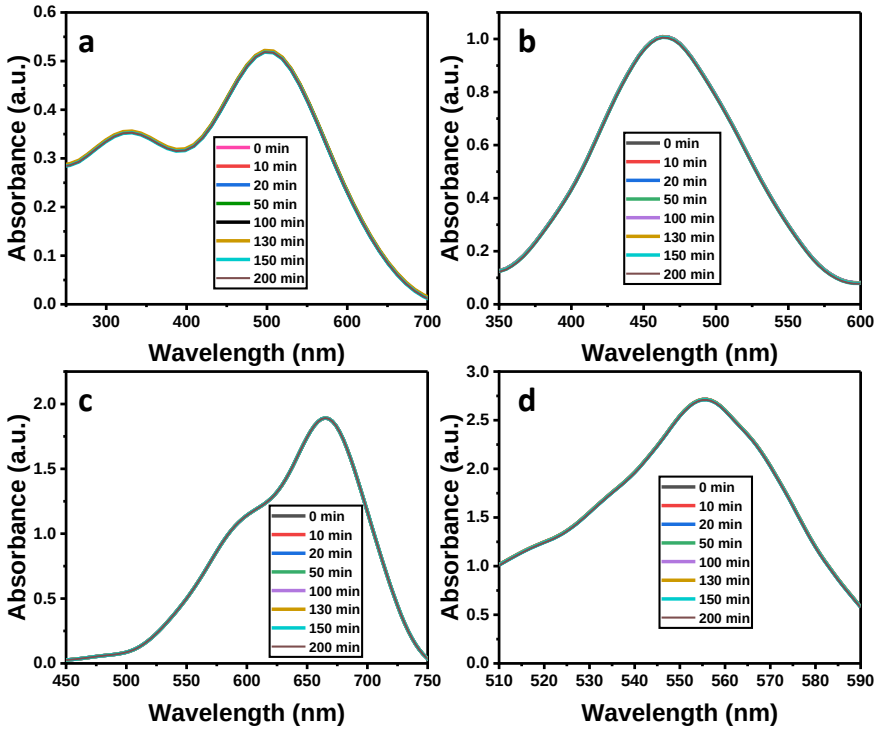

Figure 4.16: Photolysis of dyes under sunlight irradiation (a) CR (b) MO (c)MB and, (d) RhB

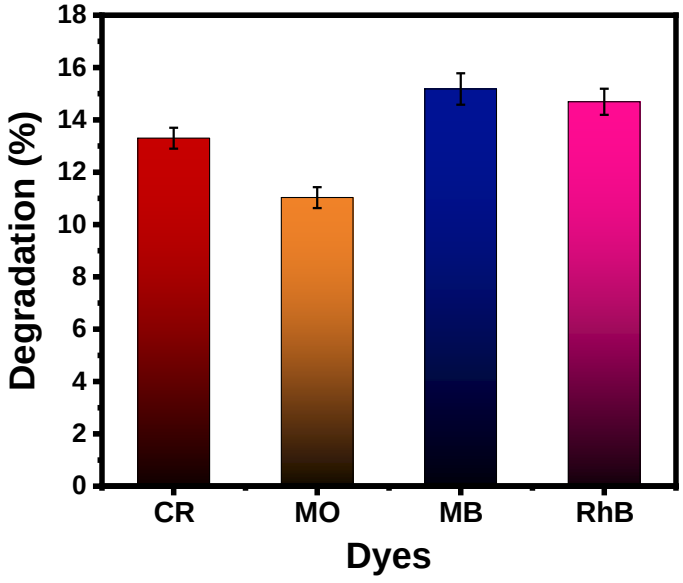

Figure 4.17: Degradation of various organic dyes using the $NaBH_4$ as the reducing agent.

The results also indicated that the dye concentration declined with increasing the sunlight irradiation time (t) in presence of $NaBH_4$. However, these organic dyes showed better degradation through photocatalytic reduction with the introduction of CuNPs dispersion in the systems. The influence of CuNPs dosages (1, 2, 3, 4, 5, and 6 mL) on the dyes degradation was investigated in the form of degradation percentage. Figure 4.18 shows the plot of CuNPs dosages versus the percentage degradation of dyes. The % degradation of CR, MO, MB, and RhB varies in the range of 42.2-88.1 %, 40.1-88.2 %, 38.5-87.0 %, and 34.2-87.0 %, respectively, as dosage increases from 1 mL to 6 mL. Results clearly showed that the degradation of dyes was almost similar after the 4 mL dosage. Therefore, a dosage of 4 mL of CuNPs dispersion has been taken as an optimized dose in further studies of the degradation of these dyes using fabricated CuNPsF7 dispersion.

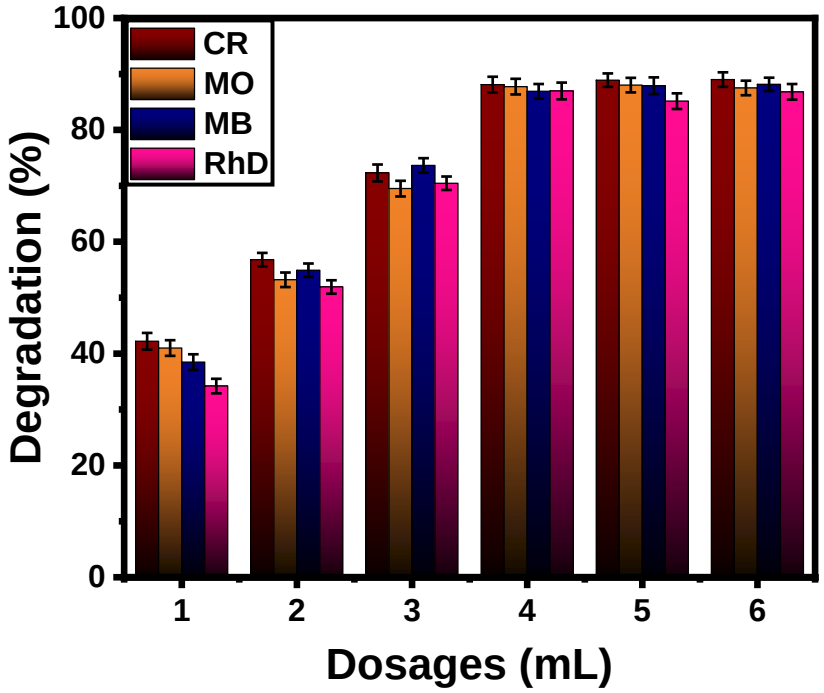

Figure 4.18: Variation in percent degradation of organic dyes at different dosages of 50 mL blank CuNPs solutions.

After the investigation of the potency of blank CuNPs for the degradation of common textile dyes, we further experimented with the photocatalytic activities of the CuNPsF7 under the optimum conditions. The degradation of four dyes was monitored using a UV-Vis spectrophotometer in the presence of CuNPsF7 dispersion.

Here, general observations found that the color changes with increasing sunlight irradiation time up to 200 min for blank CuNPs were drastically reduced up to 90 minin case of CuNPsF7 dispersion for all the dyes investigations. The irradiation time dependent photocatalytic reduction for all the dyes using copper nanoparticles clearly proves the photocatalytic hazardous dyes degradation. Also, the degradation kinetics of these dyes was quantitatively measured using the following pseudo-first-order kinetic equation (2).

$$\ln(C_t/C_0) = -K_{app}t \text{---------- (2)}$$

where C_t is the remaining dye concentration after sunlight irradiation for time t, C_0 is the initial dye concentration at zero time (i.e., before sun light irradiation), and K_{app} are the pseudo-first-order rate constant (min^{-1}).

Figure 4.19(a & b) shows the UV-visible spectra of an anionic CR dye measured at regular intervals after photocatalytic sunlight irradiation for a continuous 200 min in the presence of blank CuNPs and CuNPsF7 dispersion. The CR showed the presence of the azo linkage with a major absorption peak at 497 nm and the naphthalene rings with a minor absorption peak at 330.78 nm [78]. No other absorbance peak was found during the sunlight irradiation, which confirms the absence of any derivatives formed between CR dye and CuNPsF7 during the reaction. The decrease in the intensity of the absorption band for CR dye confirms their photocatalytic reduction, which ultimately leads to degradation.

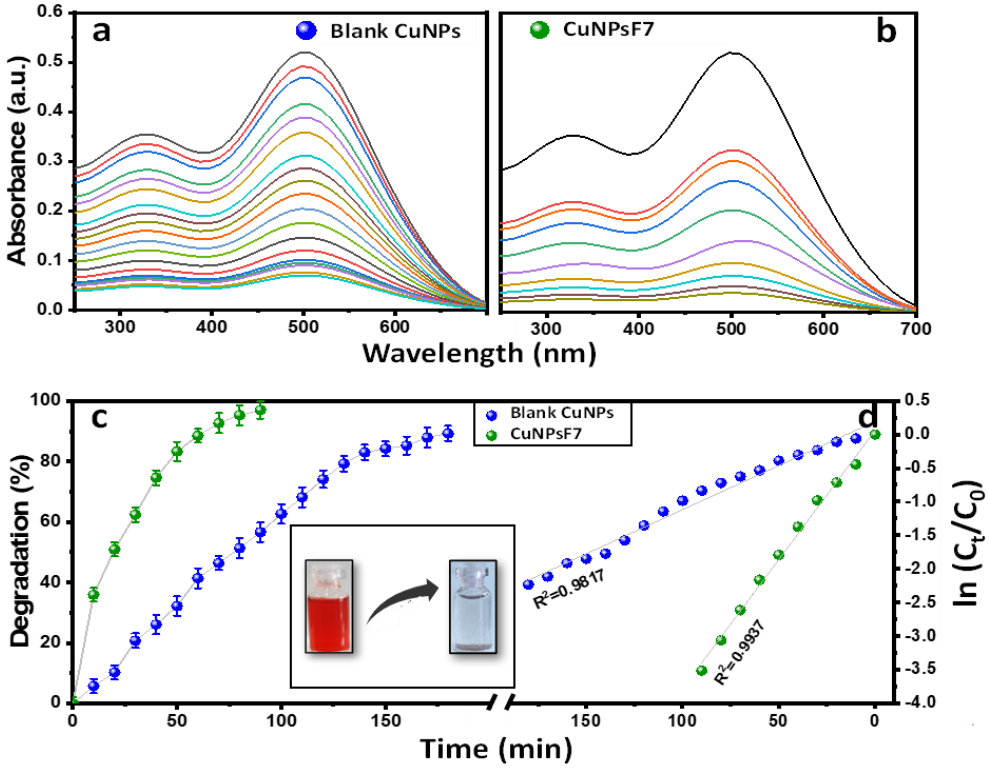

Figure 4.19: (a) UV-Vis spectra of CR dye degradation using blank CuNPs, (b) UV-Vis spectra of CR dye degradation using CuNPsF7, (c) % Degradation comparison of CR dye, (d) Kinetic study of photodegradation of CR (Insert image indicates the CR dye degradation)

It is clearly observed from Figure 4.19 that the reduction in the absorbance band of CR dye is found more in CuNPsF7 compared to blank CuNPs. It is because of the small particle size (12.70 nm), high surface area, and micellar stabilization through Pluronic F127. Figure 4.19(c) presents the plot of irradiation time versus CR dye degradation percentage. The reduction of the absorption peak at 497 nm was considered here for the evaluation of the degradation percentage in the presence of CuNPs. As shown in Figure 4.19(c), the degradation percentage of the CR dye increased with irradiation time due to the breaking of azo linkages. The blank CuNPs showed 89.28 % photocatalytic degradation at 180 min irradiation time, while almost 98.0 % dye degradation at only 90 min irradiation time was found with the CuNPsF7 dispersion. Results indicate the high amount of CR dye degradation at very quick time by CuNPsF7 dispersion because of the homogeneously dispersed copper nanoparticles as photocatalysts in the reaction. Kinetics parameters were presented in Figure 4.19(d) as the plot of $\ln(C_t/C_0)$ versus sunlight irradiation time (t) for the degradation of CR dye in the presence of blank CuNPs and CuNPsF7 dispersion. Both the blank CuNPs and CuNPsF7 confirmed the pseudo-first-order kinetics. All

the values related to the degradation and kinetics of organic dyes is listed in Table 4.3. The rate constants (k) for CuNPs and CuNPsF7 were 0.0131 and 0.0384 min^{-1}, respectively.

Results demonstrate that the CuNPsF7 dispersion as the photocatalysts delivered a high rate constant and the lowest half-life in comparison to blank CuNPs, and such a conclusion is due to the smallest particle size of 12.70 nm, better surface area, and stable photocatalytic efficiency as micellar solutions dispersed in the system with better homogeneity to face maximum dye molecules to reduce or degrade in the reaction.

Table 4.3: Percentage degradation and degradation kinetics parameters of the studied organic dyes using blank CuNPs and CuNPsF7 dispersions.

Dyes	Nanoparticles	Degradation (%)	Pseudo-first order (R^2)	Rate constant (min^{-1})	Half life
CR	Blank CuNPs	89.28	0.9817	0.0131	52.9771
	CuNPsF7	98.01	0.9937	0.0384	18.0594
MO	Blank CuNPs	86.46	0.9887	0.0131	53.0554
	CuNPsF7	96.77	0.9813	0.0320	21.7167
MB	Blank CuNPs	86.33	0.9933	0.0116	56.8496
	CuNPsF7	97.90	0.9917	0.0320	21.6895
RhB	Blank CuNPs	88.39	0.9708	0.0135	51.2372
	CuNPsF7	98.52	0.9891	0.0407	17.0561

In line with CR dye, other anionic azo dyes, such as MO, are also examined for degradation with the fabricated blank and CuNPsF7 dispersions. As shown in Figure 4.20(a & b), the MO showed absorbance maxima peak of azo linkage only at 465 nm with both the CuNPs dispersions [79]. As the potent photocatalyst, the reduction in absorbance peak of MO dye is found more in CuNPsF7 compared to blank CuNPs. As shown in Figure 4.20(c), the degradation percentage of the MO dye increased with time due to the reduction of the azo (-N=N-) bond into a corresponding amine (-NH-NH-) bond.

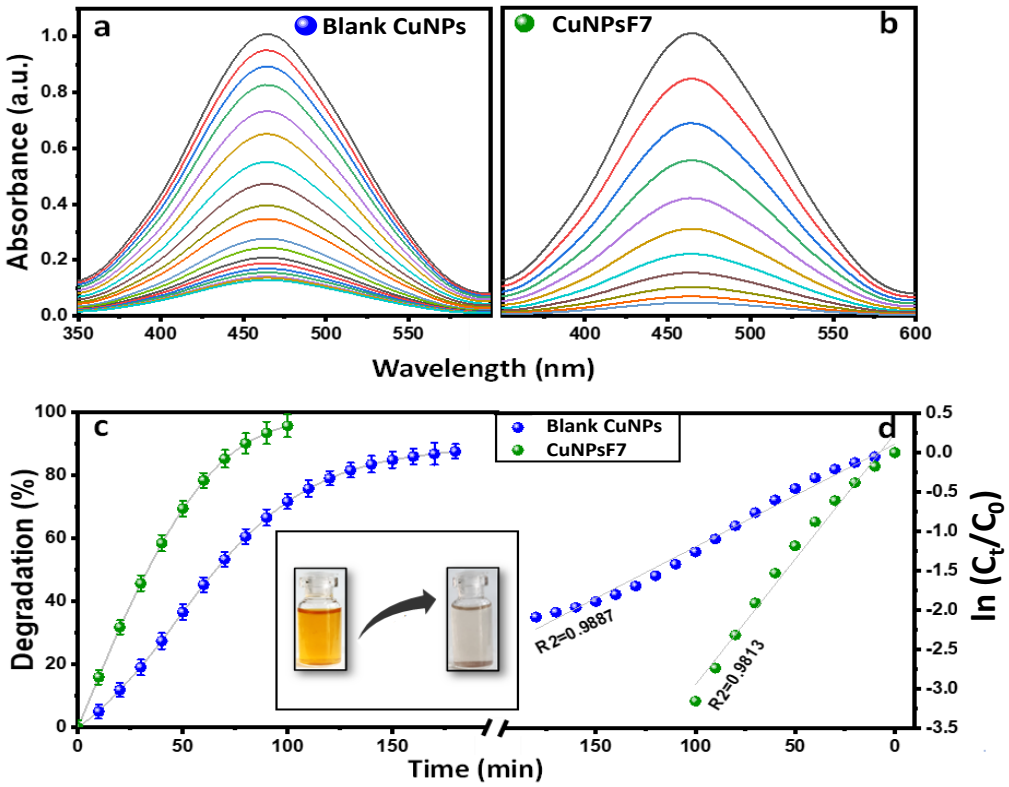

Figure 4.20: (a) UV-Vis spectra of MO dye degradation using blank CuNPs, (b) UV-Vis spectra of MO dye degradation using CuNPsF7, (c) % Degradation comparison of MO dye, (d) Kinetic study of photodegradation of MO (Insert image indicates the MO dye degradation)

The blank CuNPs showed 86.46 % degradation at 180 min, while 96.77 % dye degradation at only 100 min was given by CuNPsF7 dispersion for MO dye. It indicates the higher amount of MO dye degradation in a short time by CuNPsF7. The plot of $\ln(C_t/C_0)$ versus sunlight irradiation time (t) for the degradation of anionic MO dye in the presence of blank CuNPs and CuNPsF7 (shown in Figure 4.20(d)) showed the pseudo-first-order kinetics. The rate constants (k) of 0.0131 and 0.0320 min^{-1} were found for CuNPs and CuNPsF7 dispersions, respectively. All other parameters prove the better photocatalytic activity of CuNPsF7 dispersion for MO dye degradation.

After we looked into two anionic dyes, we further investigated how two cationic dyes (MB and RhB dyes) degraded so that CuNPsF7 dispersion could be used as a potent photocatalyst. Figure 4.21 shows the UV-visible spectra, degradation percentage, and reaction kinetics of cationic MB dye in the presence of blank CuNPs and CuNPsF7 dispersions.

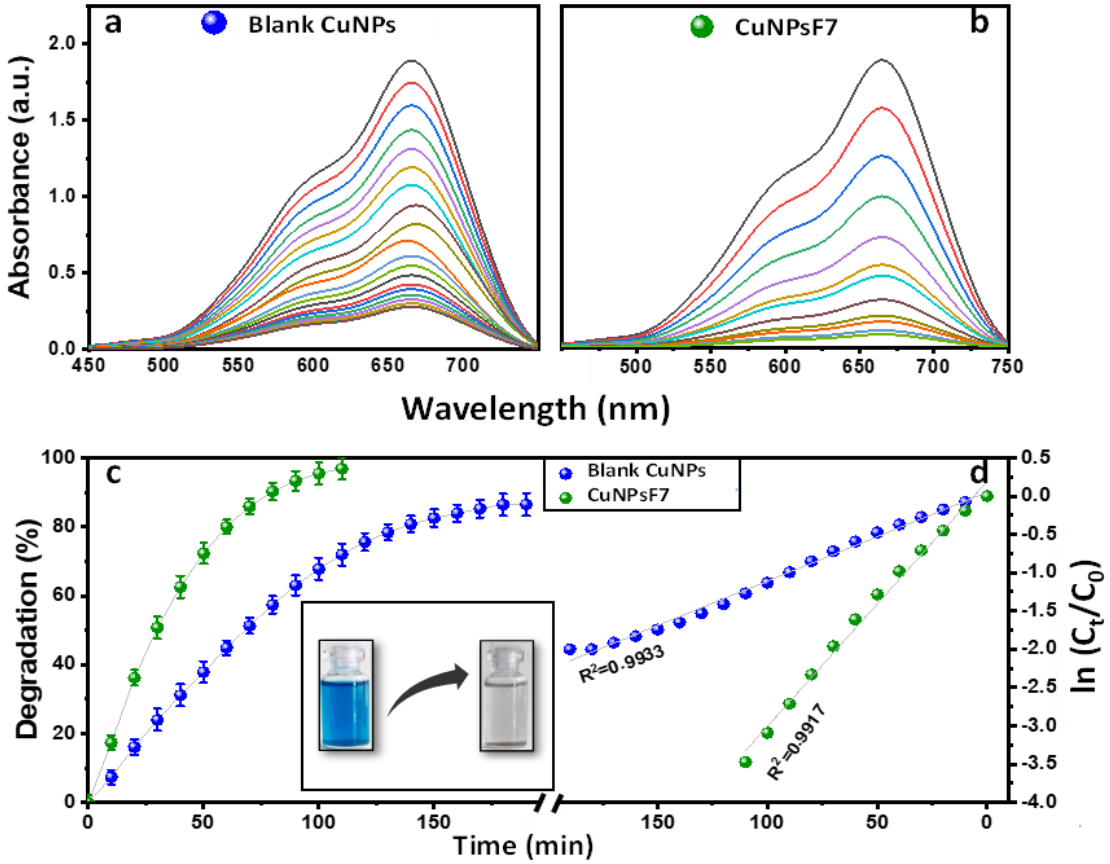

Figure 4.21: (a) UV-Vis spectra of MB dye degradation using blank CuNPs, (b) UV-Vis spectra of MB dye degradation using CuNPsF7, (c) % Degradation comparison of MB dye, (d) Kinetic study of photodegradation of MB (Insert image indicates the MB dye)

The MB showed a peak at 665 nm [79]. No other absorbance peak was examined, which indicates the absence of any other derivatives formed between MB dye and CuNPsF7 dispersion during the reaction. It is clearly observed that the reduction in absorbance band of MB dye is high in CuNPsF7 compared to blank CuNPs. As shown in Figure 4.21(c), the degradation percentage of the MB dye increased with irradiation time due to breakage of the conjugated system of the N-S heterocycle group, then the resultant hydrocarbons were oxidized and mineralized into small-molecule products, which finally degraded as CO_2 and H_2O through a series of reactions. The blank CuNPs showed 86.33% photocatalytic degradation at 190 min irradiation time for MB dye, while almost 97.90% dye degradation at only 110 min irradiation time was found with the CuNPsF7 dispersion. It indicates the high amount of MB dye degradation at very quick time by CuNPs in the presence of Pluronic F127, which confirms the

better photocatalytic reactivity of Pluronic mediated CuNPs. It shows that the degradation patterns of MB dye using both CuNPs and CuNPsF7 fit well with the pseudo-first-order kinetics (Figure 4.21(d)). The rate constants (k) of 0.0116 and 0.0320 min^{-1} were evaluated for CuNPs and CuNPsF7, respectively. This indicates similar observations found with anionic dyes. Similarly, the degradation of RhB dye using blank CuNPs and CuNPsF7 dispersion was also investigated. The cationic RhB showed a peak at 555 nm, and its intensity decreased with time (shown in Figure 4.22(a & b)) confirms their photocatalytic reduction and degradation [80].

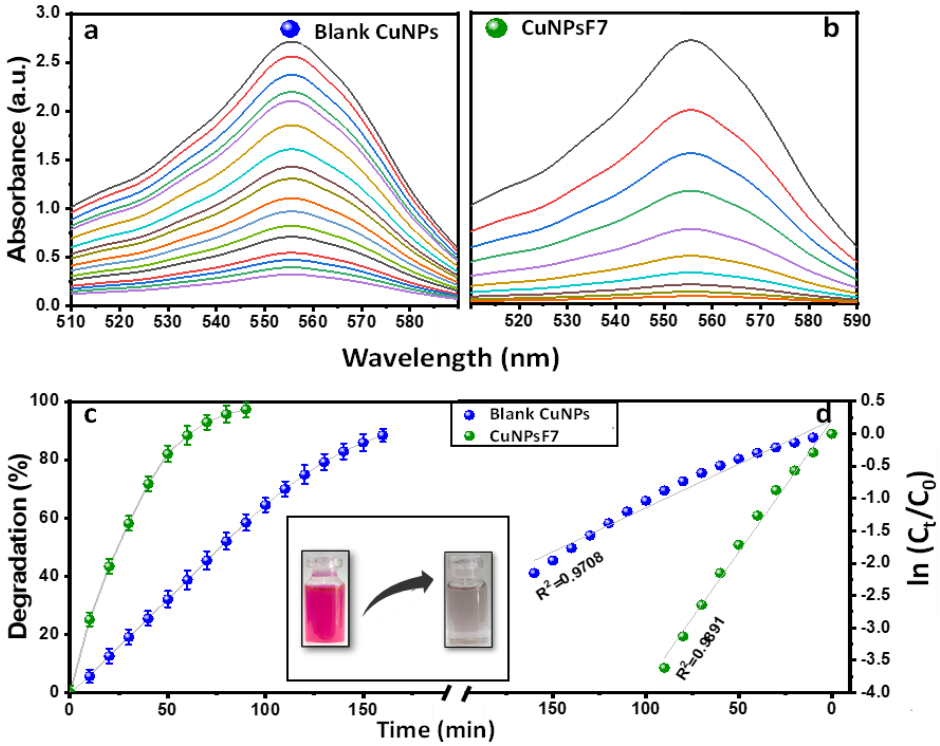

Figure 4.22: (a) UV-Vis spectra of RhB dye degradation using blank CuNPs, (b) UV-Vis spectra of RhB dye degradation using CuNPsF7, (c) % Degradation comparison of RhB dye, (d) Kinetic study of photodegradation of RhB (Insert image indicates of RhB dye degradation)

Likewise, for cationic MB dyes, the reduction in absorbance band of RhB dye is found more in CuNPsF7 dispersion. The % degradation percentage of the dye enhanced with irradiation time because of the destruction of the conjugated hetero O in the anthracene ring in the RhB molecule, which is shown in Figure 4.22(c). The blank CuNPs showed 88.39 % degradation at 160 min, while 98.52 % degradation at only 90 min was observed with the CuNPsF7. The plot shown in Figure 4.22(d) shows that the degradation of cationic RhB dye in the presence of blank CuNPs and CuNPsF7 dispersions followed pseudo-first-order kinetics. Overall, the results of the

reduction and degradation of the studied two anionic (CR and MO) and two cationic (MB and RhB) dyes confirm the potency of CuNPsF7 dispersion as a photocatalyst application in textile industry effluents.

As per our results and CuNPsF7 performance as the photocatalyst, we proposed reaction mechanism (shown in Figure 4.23) behind the photocatalytic degradation of studied dyes and it is found that the reaction occurs at the surface of the CuNPs by a Langmuir-Hinshel wood kinetics model [81].

The first step consists of the adsorption of ions as well as dye molecules on the CuNPs surface. Also, the stabilizing or capping agent, here Pluronic F127 has a potent impact and could change the reactive surface site availability frequently, thereby improving the photocatalytic activity of nanoparticles [82]. Ng et al. [83] Electron affinity is an important parameter for photocatalytic degradation of reactive textile dyes because the ionic nature or presence of lone pair electrons in the polymeric chain backbone acts as a chelating agent to stabilize the synthesized nanoparticles. Such changes were clearly found in the results of the photocatalytic activity of Pluronic mediated CuNPs compared with blank CuNPs. Here, dye reduction through Pluronic mediated CuNPs was notably enhanced compared to non-protected CuNPs. The degradation of dyes was done because sunlight irradiation changes the valence band to the conducting band of CuNPs owing to the SPR effect, gets photoexcited, and undergoes plasmonic decay, producing electron-hole pairs [84]. The interactions between the negative electrons and the electron-hole pairs were responsible for creating superoxide anion radicals and hydroxyl radical ($HO^{\bullet}$) using aerial oxygen and water molecules. Such active superoxide anion radicals and hydroxyl radicals ($HO^{\bullet}$) species created through CuNPsF7 are strongly attacked to the adsorbed dye molecules on the nanoparticle surface, which finally breakdown the dye molecule into the small molecules CO_2 and H_2O (shown in Figure 4.23) [85,86]. Not only, but the powerful adsorption capacity of CuNPsF7 facilitated the faster degradation of these dyes.

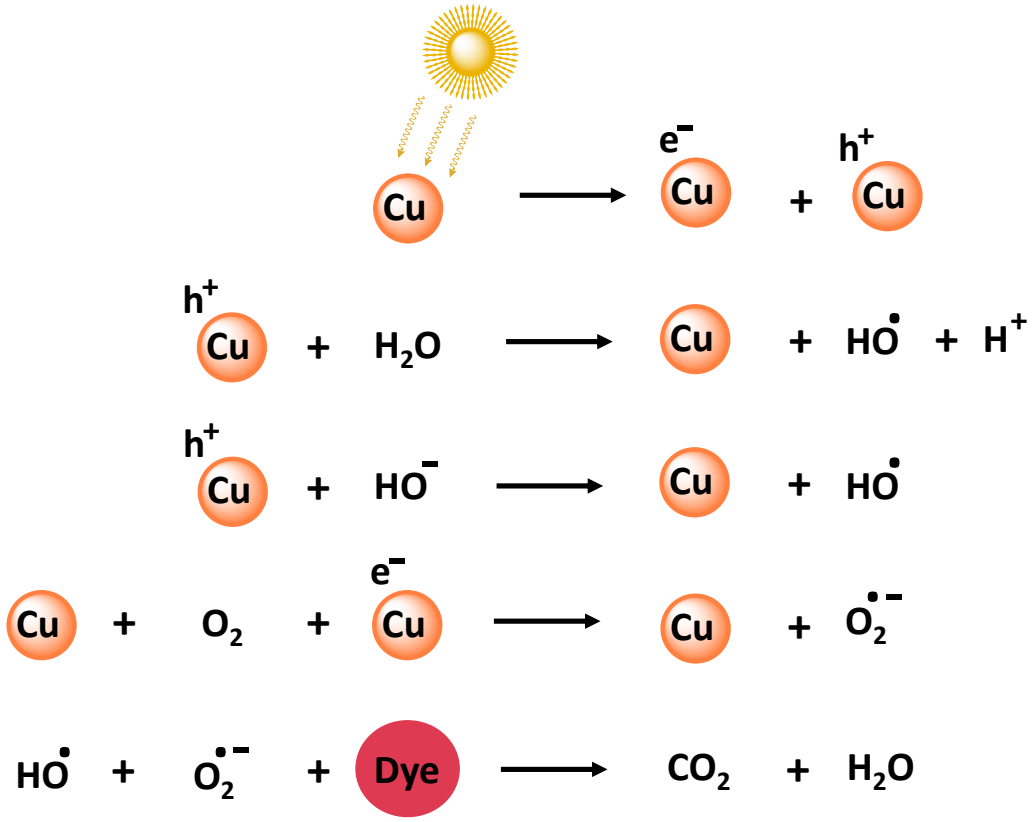

Figure 4.23: Proposed mechanism of the degradation of organic dyes in the presence of Pluronic mediated CuNPs.

Therefore, the present study clearly showed that CuNPsF7 will be the potent photocatalyst for their application in waste water treatment and the removal of toxic dyes.

It was clearly understood that the development of CuNPs using Pluronic micellar solutions through microwave-assisted techniques would be the most fruitful approach. This work opens the door to the photocatalytic activity of CuNPs in any aqueous or nonaqueous medium because of the Pluronic micellar dispersion, which can apply to any form of the system. As the purity of copper nanoparticles is enhanced by the stabilizing agent of Pluronic micelles, such nanoparticles can be used for a variety of purposes, including drug delivery, sensing, and catalysis. The use of polymermediated metal nanoparticles can provide a sustainable and effective method for the removal of dyes from wastewater, reducing their harmful impact on the environment and human health.

4.4: References

1. Czaja, A.U., Trukhan, N. and Müller, U., 2009. Industrial applications of metal–organic frameworks. *Chemical Society Reviews*, *38*(5), pp.1284-1293.
2. Ouchi, M., Terashima, T. and Sawamoto, M., 2009. Transition metal-catalyzed living radical polymerization: toward perfection in catalysis and precision polymer synthesis. *Chemical Reviews*, *109*(11), pp.4963-5050.
3. Wachs, I.E., 2005. Recent conceptual advances in the catalysis science of mixed metal oxide catalytic materials. *Catalysis Today*, *100*(1-2), pp.79-94.
4. Campelo, J.M., Luna, D., Luque, R., Marinas, J.M. and Romero, A.A., 2009. Sustainable preparation of supported metal nanoparticles and their applications in catalysis. *ChemSusChem: Chemistry & Sustainability Energy & Materials*, *2*(1), pp.18-45.
5. Yan, N., Xiao, C. and Kou, Y., 2010. Transition metal nanoparticle catalysis in green solvents. *Coordination Chemistry Reviews*, *254*(9-10), pp.1179-1218.
6. Ran, J., Zhang, J., Yu, J., Jaroniec, M. and Qiao, S.Z., 2014. Earth-abundant cocatalysts for semiconductor-based photocatalytic water splitting. *Chemical Society Reviews*, *43*(22), pp.7787-7812.
7. Senthil, R.A., Osman, S., Pan, J., Khan, A., Yang, V., Kumar, T.R., Sun, Y., Lin, Y., Liu, X. and Manikandan, A., 2020. One-pot preparation of AgBr/α-Ag2WO4 composite with superior photocatalytic activity under visible-light irradiation. *Colloids and Surfaces A: Physicochemical and Engineering Aspects*, *586*, p.124079.
8. Tilaki, R.M., Iraji Zad, A. and Mahdavi, S.M., 2007. Size, composition and optical properties of copper nanoparticles prepared by laser ablation in liquids. *Applied Physics A*, *88*, pp.415-419.
9. Pedersen, D.B., Wang, S. and Liang, S.H., 2008. Charge-transfer-driven diffusion processes in Cu@ Cu-Oxide core− shell nanoparticles: oxidation of 3.0±0.3 nm diameter copper nanoparticles. *The Journal of Physical Chemistry C*, *112*(24), pp.8819-8826.
10. Santillán, J.M.J., Videla, F.A., Fernández van Raap, M.B., Schinca, D.C. and Scaffardi, L.B., 2013. Analysis of the structure, configuration, and sizing of Cu and Cu oxide

nanoparticles generated by fs laser ablation of solid target in liquids. *Journal of Applied Physics*, *113*(13).

11. Baruah, P.K., Sharma, A.K. and Khare, A., 2018. Effective control of particle size, surface plasmon resonance and stoichiometry of Cu@ CuxO nanoparticles synthesized by laser ablation of Cu in distilled water. *Optics & Laser Technology*, *108*, pp.574-582.
12. Gawande, M.B., Goswami, A., Felpin, F.X., Asefa, T., Huang, X., Silva, R., Zou, X., Zboril, R. and Varma, R.S., 2016. Cu and Cu-based nanoparticles: synthesis and applications in catalysis. *Chemical reviews*, *116*(6), pp.3722-3811.
13. Theerthagiri, J., Chandrasekaran, S., Salla, S., Elakkiya, V., Senthil, R.A., Nithyadharseni, P., Maiyalagan, T., Micheal, K., Ayeshamariam, A., Arasu, M.V. and Al-Dhabi, N.A., 2018. Recent developments of metal oxide based heterostructures for photocatalytic applications towards environmental remediation. *Journal of Solid State Chemistry*, *267*, pp.35-52.
14. Kim, Y.H., Kang, Y.S., Lee, W.J., Jo, B.G. and Jeong, J.H., 2006. Synthesis of Cu nanoparticles prepared by using thermal decomposition of Cu-oleate complex. *Molecular Crystals and Liquid Crystals*, *445*(1), pp.231-521.
15. Zhang, Q.L., Yang, Z.M., Ding, B.J., Lan, X.Z. and Guo, Y.J., 2010. Preparation of copper nanoparticles by chemical reduction method using potassium borohydride. *Transactions of Nonferrous Metals Society of China*, *20*, pp.s240-s244.
16. Liu, Q.M., Yasunami, T., Kuruda, K. and Okido, M., 2012. Preparation of Cu nanoparticles with ascorbic acid by aqueous solution reduction method. *Transactions of Nonferrous Metals Society of China*, *22*(9), pp.2198-2203.
17. Jian-guang, Y.A.N.G., Takeshi, O., Ryoichi, I., Takeshi, B., Shigeru, S. and Masazumi, O., 2006. A Simple Way for Preparing Antioxidation Nano-copper Powders. *Chemistry Letters*, *35*(6), pp.648-649.
18. Liu, Z. and Bando, Y., 2003. A novel method for preparing copper nanorods and nanowires. *Advanced Materials*, *15*(4), pp.303-305.
19. Zhu, H., Zhang, C. and Yin, Y., 2005. Novel synthesis of copper nanoparticles: influence of the synthesis conditions on the particle size. *Nanotechnology*, *16*(12), p.3079.

20. Nakamura, T., Tsukahara, Y., Sakata, T., Mori, H., Kanbe, Y., Bessho, H. and Wada, Y., 2007. Preparation of monodispersed Cu nanoparticles by microwave-assisted alcohol reduction. *Bulletin of the Chemical Society of Japan*, *80*(1), pp.224-232.
21. Lisiecki, I. and Pileni, M.P., 1993. Synthesis of copper metallic clusters using reverse micelles as microreactors. *Journal of the American Chemical Society*, *115*(10), pp.3887-3896.
22. Yousef, S., Tatariants, M., Makarevičius, V., Lukošiūtė, S.I., Bendikiene, R. and Denafas, G., 2018. A strategy for synthesis of copper nanoparticles from recovered metal of waste printed circuit boards. *Journal of cleaner production*, *185*, pp.653-664.
23. Njoki, P.N., Rhoades, A.E. and Barnes, J.I., 2020. Microwave-Assisted synthesis of Anisotropic copper–silver nanoparticles. *Materials Chemistry and Physics*, *241*, p.122348.
24. Reverberi, A.P., Salerno, M., Lauciello, S. and Fabiano, B., 2016. Synthesis of copper nanoparticles in ethylene glycol by chemical reduction with vanadium (+ 2) salts. *Materials*, *9*(10), p.809.
25. Kumar, N. and Upadhyay, L.S.B., 2016. Facile and green synthesis of highly stable l-cysteine functionalized copper nanoparticles. *Applied Surface Science*, *385*, pp.225-233.
26. Tan, K.S. and Cheong, K.Y., 2013. Advances of Ag, Cu, and Ag–Cu alloy nanoparticles synthesized via chemical reduction route. *Journal of nanoparticle research*, *15*, pp.1-29.
27. El-Berry, M.F., Sadeek, S.A., Abdalla, A.M. and Nassar, M.Y., 2021. Microwave-assisted fabrication of copper nanoparticles utilizing different counter ions: An efficient photocatalyst for photocatalytic degradation of safranin dye from aqueous media. *Materials Research Bulletin*, *133*, p.111048.
28. Sreeju, N., Rufus, A. and Philip, D., 2016. Microwave-assisted rapid synthesis of copper nanoparticles with exceptional stability and their multifaceted applications. *Journal of Molecular Liquids*, *221*, pp.1008-1021.
29. Blosi, M., Albonetti, S., Dondi, M., Martelli, C. and Baldi, G., 2011. Microwave-assisted polyol synthesis of Cu nanoparticles. *Journal of Nanoparticle Research*, *13*, pp.127-138.
30. Wang, T.T., Chai, F., Wang, C.G., Li, L., Liu, H.Y., Zhang, L.Y., Su, Z.M. and Liao, Y., 2011. Fluorescent hollow/rattle-type mesoporous Au@ SiO2 nanocapsules for drug

delivery and fluorescence imaging of cancer cells. *Journal of colloid and interface science*, *358*(1), pp.109-115.

31. Ma, M., Chen, H., Chen, Y., Wang, X., Chen, F., Cui, X. and Shi, J., 2012. Au capped magnetic core/mesoporous silica shell nanoparticles for combined photothermo-/chemo-therapy and multimodal imaging. *Biomaterials*, *33*(3), pp.989-998.
32. Zhu, L., Wang, H., Shen, X., Chen, L., Wang, Y. and Chen, H., 2012. Developing mutually encapsulating materials for versatile syntheses of multilayer metal-silica-polymer hybrid nanostructures. *Small (Weinheim an der Bergstrasse, Germany)*, *8*(12), pp.1857-1862.
33. Xing, H., Bu, W., Zhang, S., Zheng, X., Li, M., Chen, F., He, Q., Zhou, L., Peng, W., Hua, Y. and Shi, J., 2012. Multifunctional nanoprobes for upconversion fluorescence, MR and CT trimodal imaging. *Biomaterials*, *33*(4), pp.1079-1089.
34. Chi, F., Guo, Y.N., Liu, J., Liu, Y. and Huo, Q., 2010. Size-tunable and functional core− shell structured silica nanoparticles for drug release. *The Journal of Physical Chemistry C*, *114*(6), pp.2519-2523.
35. Tepale, N., Fernández-Escamilla, V.V., Flores-Aquino, E., Sánchez-Cantú, M., Luna-Flores, A. and González-Coronel, V.J., 2019. Use of pluronic P103 triblock copolymer as structural agent during synthesis of hybrid silver nanoparticles. *Journal of Nanomaterials*, *2019*, pp.1-12.
36. Khullar, P., Singh, V., Mahal, A., Kaur, H., Singh, V., Banipal, T.S., Kaur, G. and Bakshi, M.S., 2011. Tuning the shape and size of gold nanoparticles with triblock polymer micelle structure transitions and environments. *The Journal of Physical Chemistry C*, *115*(21), pp.10442-10454.
37. Bonardd, S., Quezada, C. and Leiva, A., 2017. The role of polymers in the synthesis of noble metal nanoparticles: a review. *Journal of nanoscience and nanotechnology*, *17*(1), pp.87-114.
38. Bajpai, S.K., Mohan, Y.M., Bajpai, M., Tankhiwale, R. and Thomas, V., 2007. Synthesis of polymer stabilized silver and gold nanostructures. *Journal of nanoscience and nanotechnology*, *7*(9), pp.2994-3010.

39. Sakai, T. and Alexandridis, P., 2004. Single-step synthesis and stabilization of metal nanoparticles in aqueous pluronic block copolymer solutions at ambient temperature. *langmuir*, *20*(20), pp.8426-8430.
40. Sakai, T., Ishihara, A. and Alexandridis, P., 2015. Block copolymer-mediated synthesis of silver nanoparticles from silver ions in aqueous media. *Colloids and Surfaces A: Physicochemical and Engineering Aspects*, *487*, pp.84-91.
41. Alexandridis, P., Holzwarth, J.F. and Hatton, T.A., 1994. Micellization of poly (ethylene oxide)-poly (propylene oxide)-poly (ethylene oxide) triblock copolymers in aqueous solutions: thermodynamics of copolymer association. *Macromolecules*, *27*(9), pp.2414-2425.
42. Khullar, P., Mahal, A., Singh, V., Banipal, T.S., Kaur, G. and Bakshi, M.S., 2010. How PEO-PPO-PEO triblock polymer micelles control the synthesis of gold nanoparticles: temperature and hydrophobic effects. *Langmuir*, *26*(13), pp.11363-11371.
43. Islam, A.M. and Mukherjee, M., 2011. Effect of temperature in synthesis of silver nanoparticles in triblock copolymer micellar solution. *Journal of Experimental Nanoscience*, *6*(6), pp.596-611.
44. Alexandridis, P. and Tsianou, M., 2011. Block copolymer-directed metal nanoparticle morphogenesis and organization. *European Polymer Journal*, *47*(4), pp.569-583.
45. Jayaramudu, T., Varaprasad, K., Reddy, K.K., Pyarasani, R.D., Akbari-Fakhrabadi, A. and Amalraj, J., 2020. Chitosan-pluronic based Cu nanocomposite hydrogels for prototype antimicrobial applications. *International journal of biological macromolecules*, *143*, pp.825-832.
46. Esplugas, S., Gimenez, J., Contreras, S., Pascual, E. and Rodríguez, M., 2002. Comparison of different advanced oxidation processes for phenol degradation. *Water research*, *36*(4), pp.1034-1042.
47. Birjandi, N., Younesi, H., Bahramifar, N., Ghafari, S., Zinatizadeh, A.A. and Sethupathi, S., 2013. Optimization of coagulation-flocculation treatment on paper-recycling wastewater: application of response surface methodology. *Journal of Environmental Science and Health, Part A*, *48*(12), pp.1573-1582.

48. Zhong, P.S., Widjojo, N., Chung, T.S., Weber, M. and Maletzko, C., 2012. Positively charged nanofiltration (NF) membranes via UV grafting on sulfonated polyphenylenesulfone (sPPSU) for effective removal of textile dyes from wastewater. *Journal of Membrane Science*, *417*, pp.52-60.
49. Charumathi, D. and Das, N., 2012. Packed bed column studies for the removal of synthetic dyes from textile wastewater using immobilised dead C. tropicalis. *Desalination*, *285*, pp.22-30.
50. Tang, C. and Chen, V., 2004. The photocatalytic degradation of reactive black 5 using TiO2/UV in an annular photoreactor. *Water Research*, *38*(11), pp.2775-2781.
51. Sun, Z., Chen, Y., Ke, Q., Yang, Y. and Yuan, J., 2002. Photocatalytic degradation of a cationic azo dye by TiO2/bentonite nanocomposite. *Journal of Photochemistry and Photobiology A: Chemistry*, *149*(1-3), pp.169-174.
52. Khin, M.M., Nair, A.S., Babu, V.J., Murugan, R. and Ramakrishna, S., 2012. A review on nanomaterials for environmental remediation. *Energy & Environmental Science*, *5*(8), pp.8075-8109.
53. Tong, H., Ouyang, S., Bi, Y., Umezawa, N., Oshikiri, M. and Ye, J., 2012. Nano-photocatalytic materials: possibilities and challenges. *Advanced materials*, *24*(2), pp.229-251.
54. Nazar, N., Bibi, I., Kamal, S., Iqbal, M., Nouren, S., Jilani, K., Umair, M. and Ata, S., 2018. Cu nanoparticles synthesis using biological molecule of P. granatum seeds extract as reducing and capping agent: Growth mechanism and photo-catalytic activity. *International journal of biological macromolecules*, *106*, pp.1203-1210.
55. Mahapatra, A., Mishra, B.G. and Hota, G., 2013. Adsorptive removal of Congo red dye from wastewater by mixed iron oxide–alumina nanocomposites. *Ceramics International*, *39*(5), pp.5443-5451.
56. Afkhami, A. and Moosavi, R., 2010. Adsorptive removal of Congo red, a carcinogenic textile dye, from aqueous solutions by maghemite nanoparticles. *Journal of hazardous materials*, *174*(1-3), pp.398-403.

57. Ghorai, S., Sarkar, A.K., Panda, A.B. and Pal, S., 2013. Effective removal of Congo red dye from aqueous solution using modified xanthan gum/silica hybrid nanocomposite as adsorbent. *Bioresource technology*, *144*, pp.485-491.
58. Ai, L., Zhang, C. and Meng, L., 2011. Adsorption of methyl orange from aqueous solution on hydrothermal synthesized Mg–Al layered double hydroxide. *Journal of Chemical & Engineering Data*, *56*(11), pp.4217-4225.
59. Ai, L., Zhang, C., Liao, F., Wang, Y., Li, M., Meng, L. and Jiang, J., 2011. Removal of methylene blue from aqueous solution with magnetite loaded multi-wall carbon nanotube: kinetic, isotherm and mechanism analysis. *Journal of hazardous materials*, *198*, pp.282-290.
60. Chatterjee, S., Chatterjee, T., Lim, S.R. and Woo, S.H., 2011. Adsorption of a cationic dye, methylene blue, on to chitosan hydrogel beads generated by anionic surfactant gelation. *Environmental technology*, *32*(13), pp.1503-1514.
61. Das, S.K., Ghosh, P., Ghosh, I. and Guha, A.K., 2008. Adsorption of rhodamine B on Rhizopus oryzae: role of functional groups and cell wall components. *Colloids and Surfaces B: Biointerfaces*, *65*(1), pp.30-34.
62. Kaur, H. and Kaur, R., 2014. Removal of Rhodamine-B dye from aqueous solution onto Pigeon Dropping: adsorption, kinetic, equilibrium and thermodynamic studies. *J Mater Environ Sci*, *5*(6), pp.1830-1838.
63. Verma, A., Dwivedi, R., Prasad, R. and Bartwal, K.S., 2013. Microwave-assisted synthesis of mixed metal-oxide nanoparticles. *Journal of Nanoparticles*, *2013*.
64. Tsuji, M., Hashimoto, M., Nishizawa, Y., Kubokawa, M. and Tsuji, T., 2005. Microwave-assisted synthesis of metallic nanostructures in solution. *Chemistry–A European Journal*, *11*(2), pp.440-452.
65. Kubiak, A., Bielan, Z., Kubacka, M., Gabała, E., Zgoła-Grześkowiak, A., Janczarek, M., Zalas, M., Zielińska-Jurek, A., Siwińska-Ciesielczyk, K. and Jesionowski, T., 2020. Microwave-assisted synthesis of a TiO2-CuO heterojunction with enhanced photocatalytic activity against tetracycline. *Applied Surface Science*, *520*, p.146344.

66. Kubiak, A., Żółtowska, S., Gabała, E., Szybowicz, M., Siwińska-Ciesielczyk, K. and Jesionowski, T., 2021. Controlled microwave-assisted and pH-affected growth of ZnO structures and their photocatalytic performance. *Powder Technology*, *386*, pp.221-235.
67. Kubiak, A., Bielan, Z., Bartkowiak, A., Gabała, E., Frankowski, M., Zalas, M., Siwińska-Ciesielczyk, K., Janczarek, M. and Jesionowski, T., 2022. A novel microwave-assisted strategy to fabricate multifunctional photoactive titania-based heterostructures with enhanced activity. *Materials Research Bulletin*, *147*, p.111633.
68. Liu, K.J., 1968. Nuclear magnetic resonance studies of polymer solutions. V. Cooperative effects in the ion-dipole interaction between potassium iodide and poly (ethlene oxide). *Macromolecules*, *1*(4), pp.308-311.
69. Sakai, T. and Alexandridis, P., 2005. Mechanism of gold metal ion reduction, nanoparticle growth and size control in aqueous amphiphilic block copolymer solutions at ambient conditions. *The journal of physical chemistry B*, *109*(16), pp.7766-7777.
70. Fievet, F., Fievet-Vincent, F., Lagier, J.P., Dumont, B. and Figlarz, M., 1993. Controlled nucleation and growth of micrometre-size copper particles prepared by the polyol process. *Journal of Materials Chemistry*, *3*(6), pp.627-632.
71. Pham, N.D., Duong, M.M., Le, M.V. and Hoang, H.A., 2019. Preparation and characterization of antifungal colloidal copper nanoparticles and their antifungal activity against Fusarium oxysporum and Phytophthora capsici. *ComptesRendus. Chimie*, *22*(11-12), pp.786-793.
72. Fathima, J.B., Pugazhendhi, A., Oves, M. and Venis, R., 2018. Synthesis of eco-friendly copper nanoparticles for augmentation of catalytic degradation of organic dyes. *Journal of Molecular Liquids*, *260*, pp.1-8.
73. Azzam, E.M.S. and Zaki, M.F., 2016. Surface and antibacterial activity of synthesized nonionic surfactant assembled on metal nanoparticles. *Egyptian Journal of Petroleum*, *25*(2), pp.153-159.
74. Khan, M.B., 2017. Rheological behavior of polyacrylamide solution in the presence of cationic Gemini surfactants/conventional surfactants. *Asia-Pacific Journal of Chemical Engineering*, *12*(4), pp.671-678.

75. Hsu, B.Y.W., Teh, C., Tan, H., Wong, S.Y., Zhang, Y., Korzh, V., Li, X. and Wang, J., 2012. PEO surface-decorated silica nanocapsules and their application in in vivo imaging of zebrafish. *RSC advances*, *2*(32), pp.12392-12399.
76. Miyazawa, T., Itaya, M., Burdeos, G.C., Nakagawa, K. and Miyazawa, T., 2021. A critical review of the use of surfactant-coated nanoparticles in nanomedicine and food nanotechnology. *International journal of nanomedicine*, pp.3937-3999.
77. Zhou, R., Wu, X., Hao, X., Zhou, F., Li, H. and Rao, W., 2008. Influences of surfactants on the preparation of copper nanoparticles by electron beam irradiation. *Nuclear Instruments and Methods in Physics Research Section B: Beam Interactions with Materials and Atoms*, *266*(4), pp.599-603.
78. Fowsiya, J., Madhumitha, G., Al-Dhabi, N.A. and Arasu, M.V., 2016. Photocatalytic degradation of Congo red using Carissa edulis extract capped zinc oxide nanoparticles. *Journal of Photochemistry and Photobiology B: Biology*, *162*, pp.395-401.
79. Sithole, R.K., Machogo, L.F., Moloto, M.J., Gqoba, S.S., Mubiayi, K.P., Van Wyk, J. and Moloto, N., 2020. One-step synthesis of Cu3N, Cu2S and Cu9S5 and photocatalytic degradation of methyl orange and methylene blue. *Journal of Photochemistry and Photobiology A: Chemistry*, *397*, p.112577.
80. Shayegan Mehr, E., Sorbiun, M., Ramazani, A. and Taghavi Fardood, S., 2018. Plant-mediated synthesis of zinc oxide and copper oxide nanoparticles by using ferulagoangulata (schlecht) boiss extract and comparison of their photocatalytic degradation of Rhodamine B (RhB) under visible light irradiation. *Journal of Materials Science: Materials in Electronics*, *29*, pp.1333-1340.
81. Herves, P., Pérez-Lorenzo, M., Liz-Marzán, L.M., Dzubiella, J., Lu, Y. and Ballauff, M., 2012. Catalysis by metallic nanoparticles in aqueous solution: model reactions. *Chemical Society Reviews*, *41*(17), pp.5577-5587.
82. Ansar, S.M. and Kitchens, C.L., 2016. Impact of gold nanoparticle stabilizing ligands on the colloidal catalytic reduction of 4-nitrophenol. *ACS Catalysis*, *6*(8), pp.5553-5560.
83. Ng, L.Y., Mohammad, A.W., Leo, C.P. and Hilal, N., 2013. Polymeric membranes incorporated with metal/metal oxide nanoparticles: A comprehensive review. *Desalination*, *308*, pp.15-33.

84. Sathiyavimal, S., Vasantharaj, S., Kaliannan, T. and Pugazhendhi, A., 2020. Eco-biocompatibility of chitosan coated biosynthesized copper oxide nanocomposite for enhanced industrial (Azo) dye removal from aqueous solution and antibacterial properties. *Carbohydrate polymers*, *241*, p.116243.
85. Phul, R., Kaur, C., Farooq, U. and Ahmad, T., 2018. Ascorbic acid assisted synthesis, characterization and catalytic application of copper nanoparticles. *Mater. Sci. Eng. Int. J*, *2*(4), pp.90-94.
86. Hamadanian, M., Reisi-Vanani, A. and Majedi, A., 2010. Synthesis, characterization and effect of calcination temperature on phase transformation and photocatalytic activity of Cu, S-codoped TiO2 nanoparticles. *Applied Surface Science*, *256*(6), pp.1837-1844.